ROCK PHYSICS MODELING FOR A CLASTIC RESERVOIR IN SAUDI ARABIA

BY

OMAR HUSSEIN OMAR AFIF

A Thesis Presented to the
DEANSHIP OF GRADUATE STUDIES

KING FAHD UNIVERSITY OF PETROLEUM & MINERALS

DHAHRAN, SAUDI ARABIA

In Partial Fulfillment of the
Requirements for the Degree of

MASTER OF SCIENCE

In
GEOPHYSICS

May 2015

KING FAHD UNIVERSITY OF PETROLEUM & MINERALS

DHAHRAN- 31261, SAUDI ARABIA

DEANSHIP OF GRADUATE STUDIES

This thesis, written by Omar Hussein Omar Afif under the direction his thesis advisor and approved by his thesis committee, has been presented and accepted by the Dean of Graduate Studies, in partial fulfillment of the requirements for the degree of **MASTER OF SCIENCE IN GEOPHYSICS.**

Dr. Abdullatif A. Al-Shuhail
(Advisor)

Dr. Abdulaziz Al-Shaibani
Department Chairman

Dr. Aiman M. Bakhorji
(Co-Advisor)

Dr. Salam A. Zummo
Dean of Graduate Studies

Dr. SanLinn Ismail Kaka
(Member)

9/10/16
Date

Dr. Khalid Al-Ramadan
(Member)

Dr. Abdullah Alshuhail
(Member)

I dedicate this work to my mother who passed away during my work on this thesis, may God bless her soul. I also dedicate this thesis to my father who was the primary teacher who taught me the realities of life, may God bless his soul. Moreover, I would like to dedicate this work to my wife who was supporting, encouraging and patient throughout the work of this study, and to my children Hussein, Abdullah, and Abdulaziz who have lightened my days while I worked on this thesis.

ACKNOWLEDGMENTS

All praise to almighty ALLAH, the most Merciful and the most Benevolent, who gave me the power, chance, ability, patience and time to complete this thesis.

I am very grateful to my thesis committee: Dr. Abdullatif Al-Shuhail, my thesis advisor, Dr. SanLinn Ismail, Dr. Abdullah Al-Shuhail and Dr. Khalid Al-Ramadan from King Fahd University of Petroleum and Minerals (KFUPM), and Dr. Aiman Bakhorji, rock physicist, from Saudi Aramco for their support, ideas, guidance and constructive comments. I would also like to express my sincere acknowledgment to all faculty members, all staff of the Department of Earth Sciences at KFUPM, and all my course instructors for their individual and collective assistance.

Special thanks go to Saudi Aramco's Exploration organization members and management for their help and support, and for providing me with well log data. A special recognition is due to my colleagues Mohammad Bannagi, Mukarram Ahmed, Rudi Lubbe and Harianto Soepriatna for their technical help and support. I wish to thank Husam Mustafa and Mohammad Otaibi, Geophysical Technical Service Division (GPTSD), Saudi Aramco, for their strong management support. I take this opportunity to express my profound gratitude and deep regard to my mentor Dr. Aiman Bakhorji, who supported me, obtained Saudi Aramco approval to use its well log data, and guided and monitored my work on this thesis. I would like also to thank Mr. Mahmoud Yassin, Schlumberger, for his great contribution in showing me how to evaluate reservoir petrophysics properties. Special thanks to my colleague Ahmed Saleh Al-Ghamdi, who encouraged and supported me to enroll in the

Geophysics master's degree program at KFUPM. Grateful thanks go to all GPTSD members for their help and support.

Finally, my heartfelt appreciation is dedicated to my wife, my sons, brothers, sisters, father- and mother-in-low, and to my friends, for their words of encouragement and moral support during the course of my studies.

TABLE OF CONTENTS

LIST OF TABLES

LIST OF FIGURES

LIST OF ABBREVIATIONS AND SYMBOLS

λ	: Lambda
μ	: Mu (Shear modulus)
ϕ	: Porosity
ϕ_c	: Critical porosity
ρ	: Rho
δ	: Normal displacement
τ	: Tangential displacement
API	: American Petroleum Institute
C	: Coordination number
DIFCAL	: Differential caliper (Caliper – Bit size)
DRHO	: Density correction
E	: Young's modulus
F	: Formation factor
GR	: Gamma ray
GWLA	: Geophysical Well Log Analysis
I_{GR}	: The gamma ray shale index
Ip	: Acoustic impedance (P-impedance)
Is	: Shear impedance (S-impedance)
K	: Bulk modulus
M	: Compressional or P-modulus
MLR	: Multilinear regression
QC	: Quality control
PR	: Poisson's ratio

RHOB : Bulk density

RPT : Rock Physics Template

R_t : Measured formation resistivity

R_w : Formation water resistivity

S_h : Hydrocarbon saturation

S_n : Normal stiffnesses

S_t : Tangential stiffnesses

S_w : Water saturation

VQZ : Volume of Quartz

V_p : Compressional velocity (P-wave velocity)

V_p/V_s : Velocity ratio

V_s : Shear velocity (S-wave velocity)

VSh : Volume of Shale

ABSTRACT

Full Name : Omar Hussein Omar Afif

Thesis Title : Rock Physics Modeling for a Clastic Reservoir in Saudi Arabia

Major Field : Geophysics, Earth Science Department

Date of Degree : May 2015

Understanding seismic response at the reservoir level is a critical part of oil/gas exploration studies. The seismic response of the subsurface is determined by the spatial distribution of the elastic properties. Consequently, accurately translating elastic properties to quantitative reservoir properties such as lithology, porosity, and fluid type is required. One way to achieve this goal is through rock physics analysis and modeling.

Four well datasets, including gamma ray, density, resistivity, caliper, compressional and shear sonic logs, are used to determine a rock physics model for a clastic reservoir in Saudi Arabia. Different techniques, methods and workflows include the so-called Geophysical Well Log Analysis (GWLA) and are conducted to enhance and condition the quality of the elastic logs. The conditioned logs, with other available logs, are then combined to calculate the petrophysical properties.

Several rock physics models are compared and evaluated at the reservoir including stiff-sand (Mavko et al., 2009), soft-sand (Dvorkin and Nur, 1996), the Greenberg and Castagna (1992) and Raymer's (1980) models. The stiff-sand model proved to be the most appropriate and universal transform for the wells under examination in this study. This model is used to create and supply equations that estimate the porosity from the seismically derived impedance.

ملخص الرسالة

الاسم الكامل: عمر حسين عمر عفيف

عنوان الرسالة: نمذجة الخصائص الفيزيائية للصخور مكمن رسوبي في المملكة العربية السعودية

التخصص: جيوفيزياء – علوم الأرض

تاريخ الدرجة العلمية: مايو ٢٠١٥م

تعتبر دراسة وفهم الموجات الزلزالية من الدراسات المهمة في أعمال الاستكشاف أو التنقيب عن البترول وذلك لتحديد مواقع البترول تحت سطح الأرض. وتوجد أنواع مختلفة للموجات الزلزالية ولكل نوع خصائص مرونة تختلف من مكان لأخر حسب مكونات الصخور ونوع السائل الموجود فيها. فلهذا يجب تحليل ودراسة خصائص المرونة للموجات الزلزالية بدقة وبشكل واسع حتى يتسنى لنا ربطها بخصائص المكمن مثل المسامية أو كمية ونوع المعادن والسوائل الموجودة داخل المكمن (زيت أو غاز أو ماء). ولتحقيق ذلك لابد من عمل تحليل للخصائص الفيزيائية للصخور وعمل نماذج لها لربطها بخصائص المكمن.

خلال هذه الدراسة تم استخدام مجموعة من المعطيات والبيانات لعدد اربعة أبار بترولية في المملكة العربية السعودية. وتشمل هذه البيانات سجلات متصلة لأشعة جاما والكثافة والمقاومة النوعية وقياس التغير في محيط البئر وسجلات الموجات الزلزالية الأولية والثانوية. وتم إعداد وتصميم خطوات عمل لإنجاز هذه المهمة واستخدام عدد من التقنيات المختلفة تسمى التحليل الجيوفيزيائي لسبر الآبار. ويعمل هذا التحليل على تحسين جودة السجلات والبيانات والقياسات الجيوفيزيائية. ويتم استخدام هذه البيانات وغيرها من المعطيات المتوفرة لحساب الخصائص البترولية مثل المسامية وكميات نوع السوائل والصخور المتوفرة في المكمن هذا بالإضافة لمعرفة الخصائص الفيزيائية للمكمن.

واشتملت هذه الدراسة على اختبار عدد من النماذج الفيزيائية المتوفرة وتقيمها داخل حدود المكمن في مواقع آبار الدراسة. ومن هذه النماذج الرمل الصلب (Stiff-sand) والرمل الناعم (Soft-sand) وجريينبيرج-كستانيا (Greenberg and Castagna) بالإضافة إلى ريمير (Raymer's). وتم اختيار طريقة أو نموذج الرمل الصلب كطريقة ملائمة لربط الخصائص الفيزيائية للموجات الزلزالية بخصائص المكمن. وباستخدام هذه الطريقة تم صياغة معادلة لحساب المسامية واشتقاقها من خصائص الموجات الزلزالية.

CHAPTER 1

INTRODUCTION

1.1 Motivation

Seismic response of the subsurface is determined by the spatial distribution of the elastic properties. Consequently, accurately translating elastic properties to quantitative reservoir properties such as lithology, porosity and fluid type is needed. In quantitative seismic interpretation of the hydrocarbon reservoir, the elastic properties of the sediment must be related to the volume of hydrocarbon present. One way of achieving this goal is through rock physics modeling.

1.2 Research Objectives

The objective of this study is to establish a suitable rock physics workflow that helps to build a rock physics model for a clastic reservoir in Saudi Arabia. The study employed different rock physics models, using published empirical and theoretical approaches, to understand the logs response and relate them to the effects of porosity, lithology and fluid type.

1.3 Chapter Descriptions

Chapter 2 provides a geological overview of the studied reservoir and discusses the dataset used during this study.

Chapter 3 shows the methodology of the data conditioning and petrophysical analysis applied over the formation of interest to enhance the log data quality and to calculate the reservoir properties (e.g., shale volume, porosity, water saturation and lithology). In this chapter, the recommended workflows for applying these methodologies are designed and discussed.

Chapter 4 gives an introduction to elastic theory and to concepts of elastic bounds and fluid substitution using Gassmann model. A number of contact models are explained and tested to describe the velocity-porosity behavior of a clastic reservoir. Later, the modeled behavior is constrained by local geology to build a rock physics model and template.

The last chapter summarizes the thesis and includes recommendations for future work.

CHAPTER 2

STUDY AREA

2.1 Geology Overview

The target reservoir in this study is Unayzah, which is divided into three members: a (youngest), b, and c, (Melvin, 2010). The Unayzah-a member is unconformably bound by the marginal marine basal Khuff carbonate/clastic above. It also bounded by a quartz-cemented Unayzah-c member below, which is described as a low porosity clastic unit, (Wallick, 2013) and Unayzah-b member in the study wells is truncated. In this research, the Khuff carbonate formation is denoted by the letter A and the Unayzah-a member is denoted by the letter B. The Unayzah-a formation is highly heterogeneous and in many locations it is present as a thin layer. Therefore, it is not detectable at current seismic resolution. At the study-well locations a distinct impedance change between the carbonate and clastic rocks is clear (Figure 1). The Unayzah-a member is divided into two stratal units. The lower unit has poor reservoir quality consisting of a thin discontinuous basal eolian dune sandstone abruptly overlain by very fine-grained and silty, irregularly laminated sandstones. In the upper unit, several facies of varying reservoir quality are recognized and represented deposits laid down in a mixed eolian depositional system (Melvin, 2010).

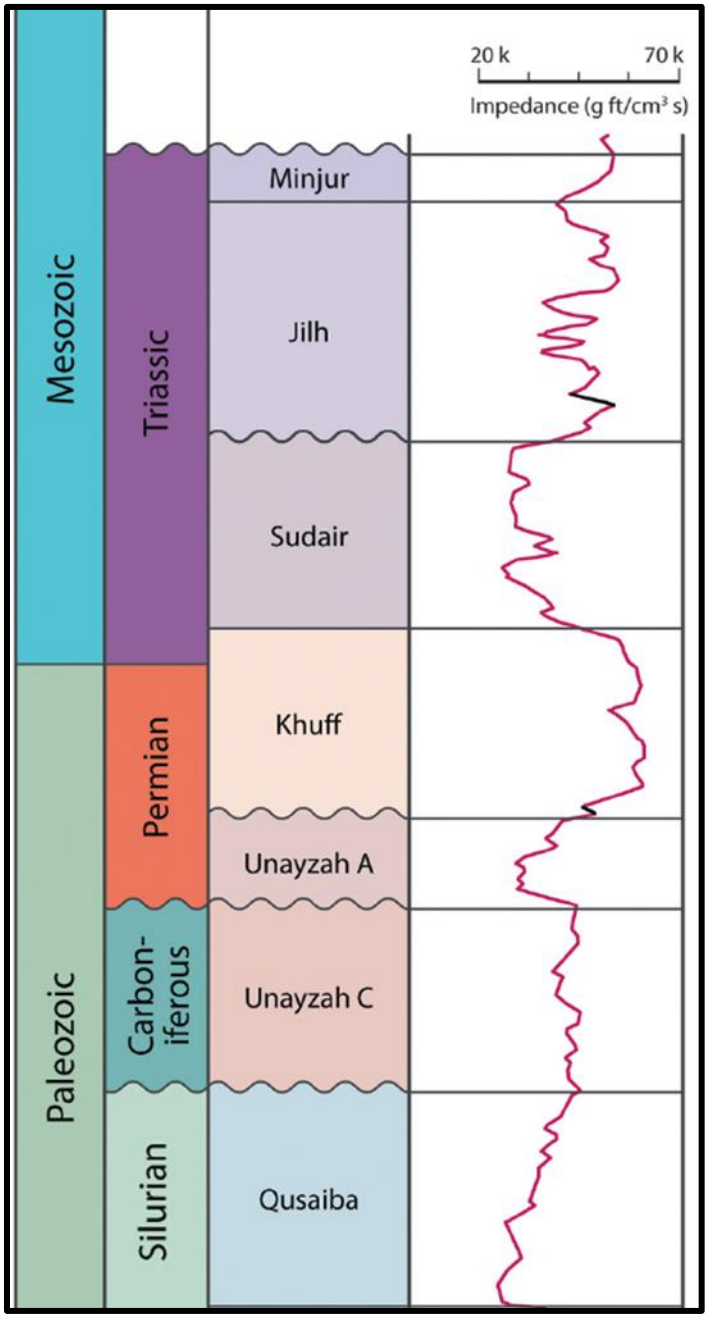

Figure 1. Geological column relating Unayzah and other stratigraphic units in the study area with a representative impedance log on the last right track (modified from Wallick, 2013).

2.2 Dataset

Four wells in the eastern part of Saudi Arabia are studied and analyzed in this thesis (Figure 2). A full suite of logs was involved and included gamma ray, density, sonic, resistivity and caliper logs (Figures 3-6).

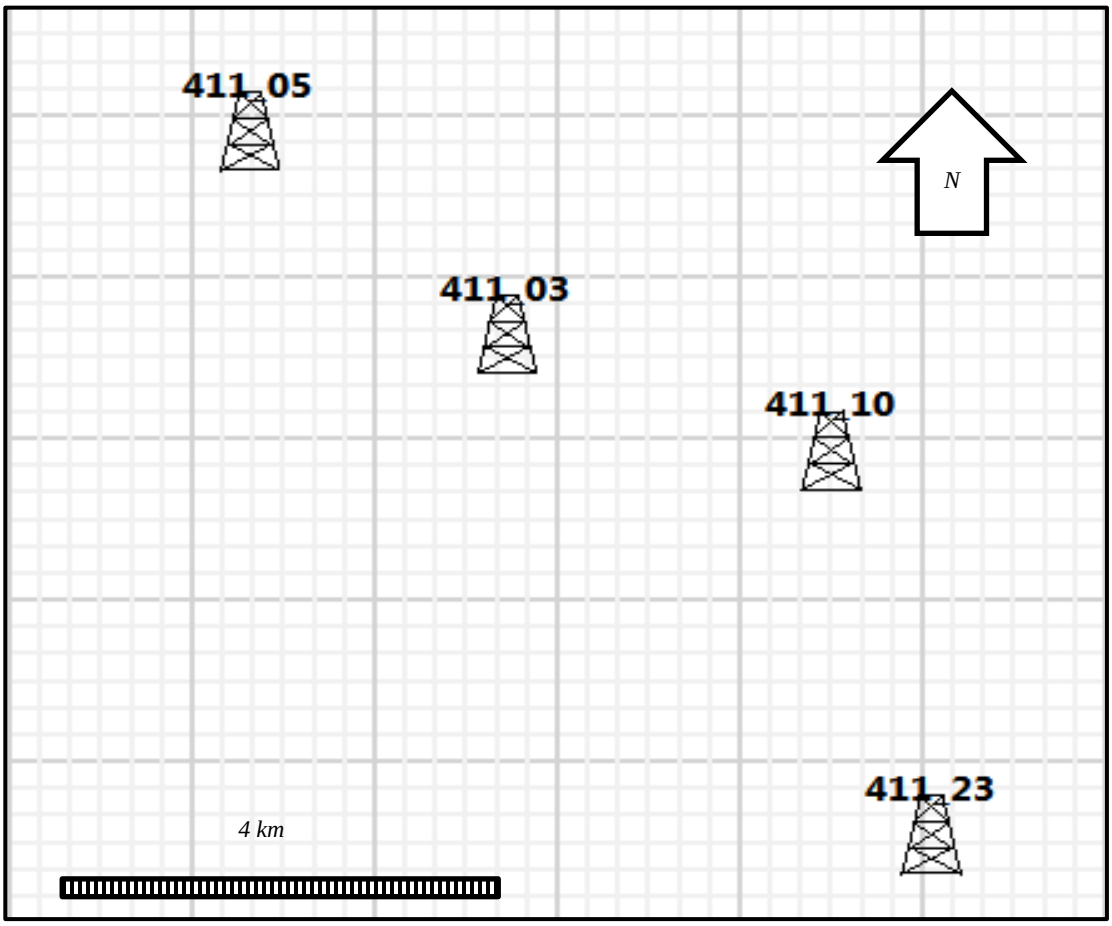

Figure 2. Relative locations of wells used in the study area.

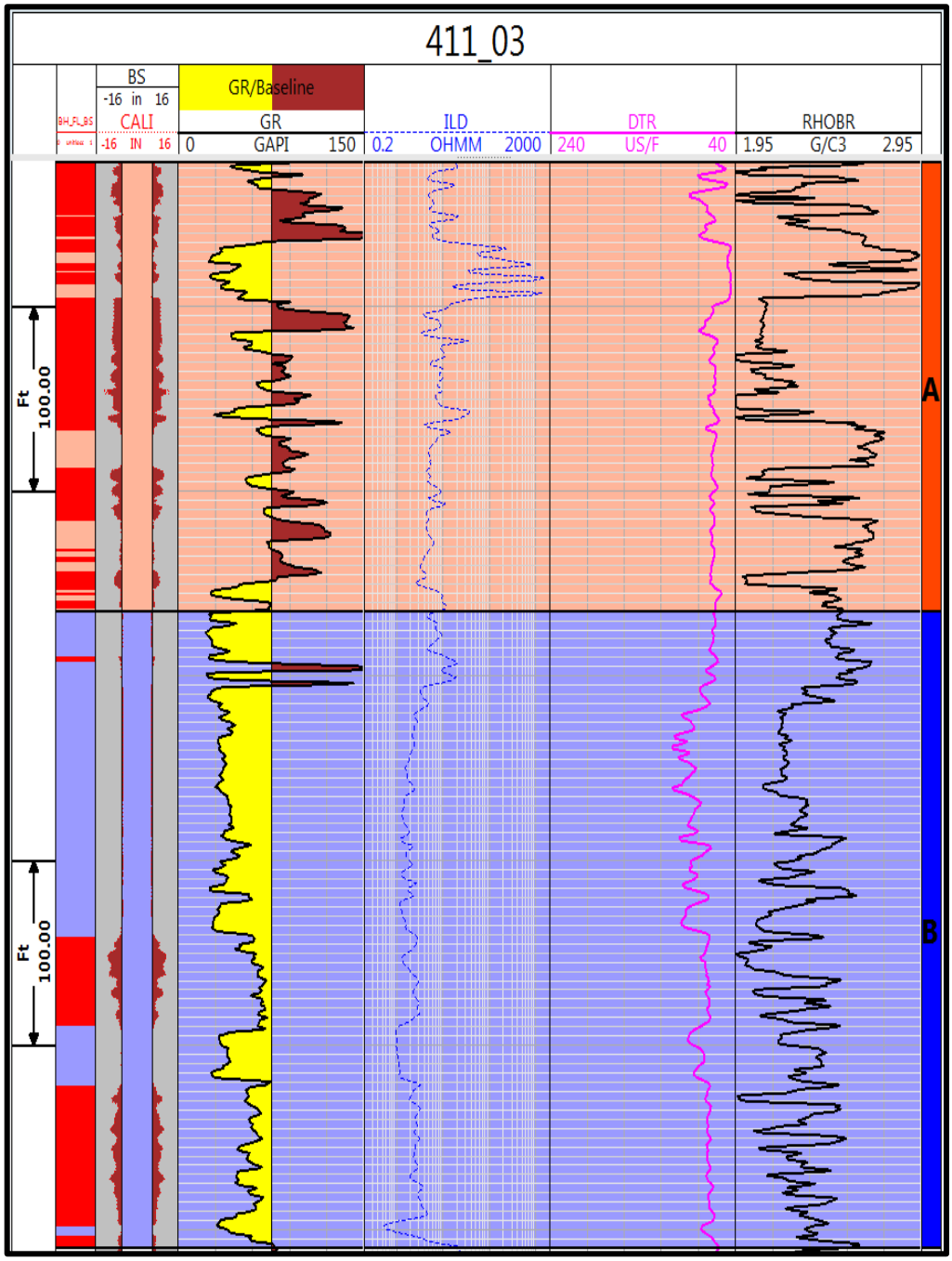

Figure 3. Logs used in this study, tracks from left to right: scale; washout flag; caliper and bit size; gamma ray; resistivity; compressional slowness; density and zones name for well 411_03.

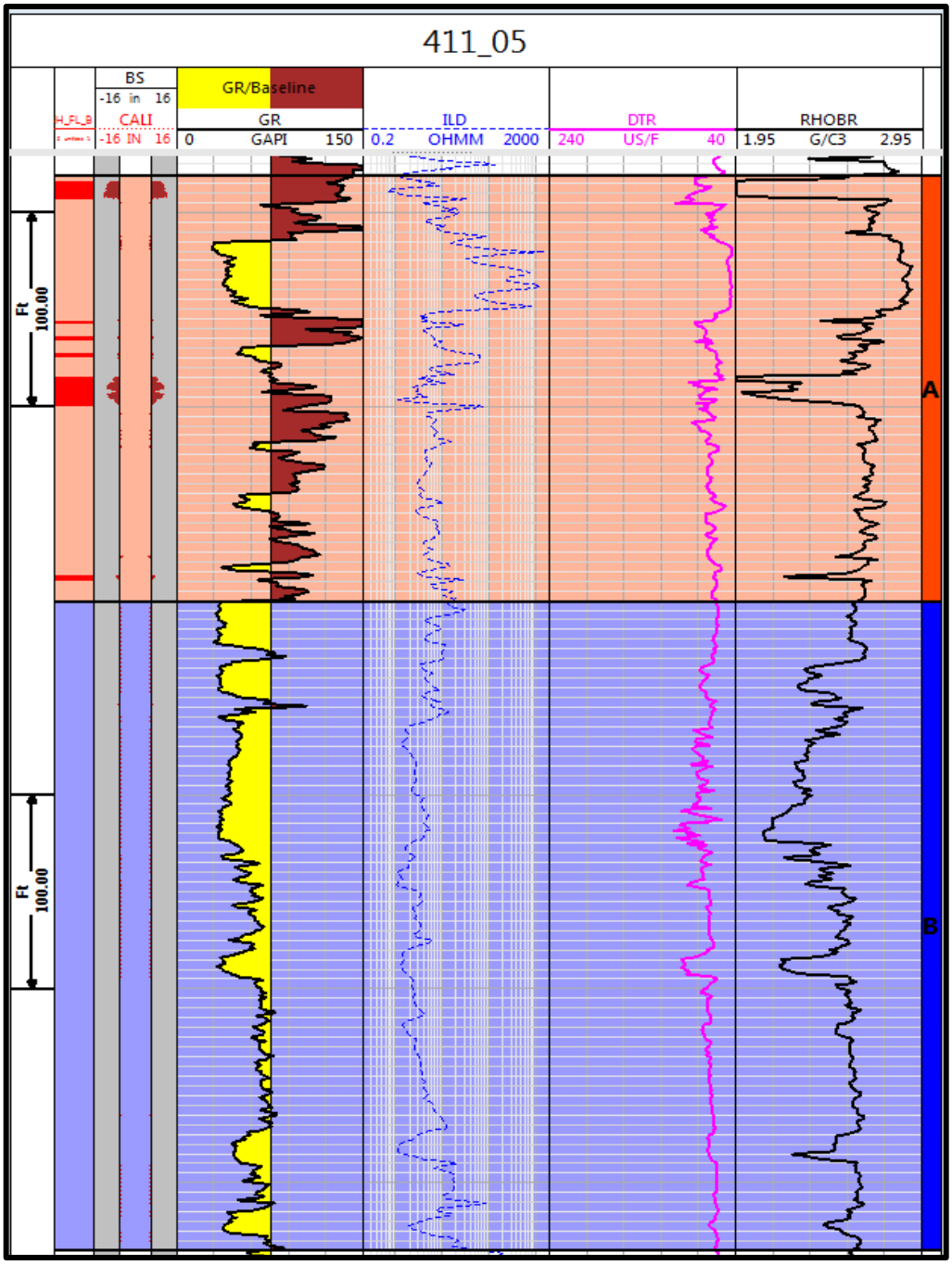

Figure 4. Logs for well 411_05.

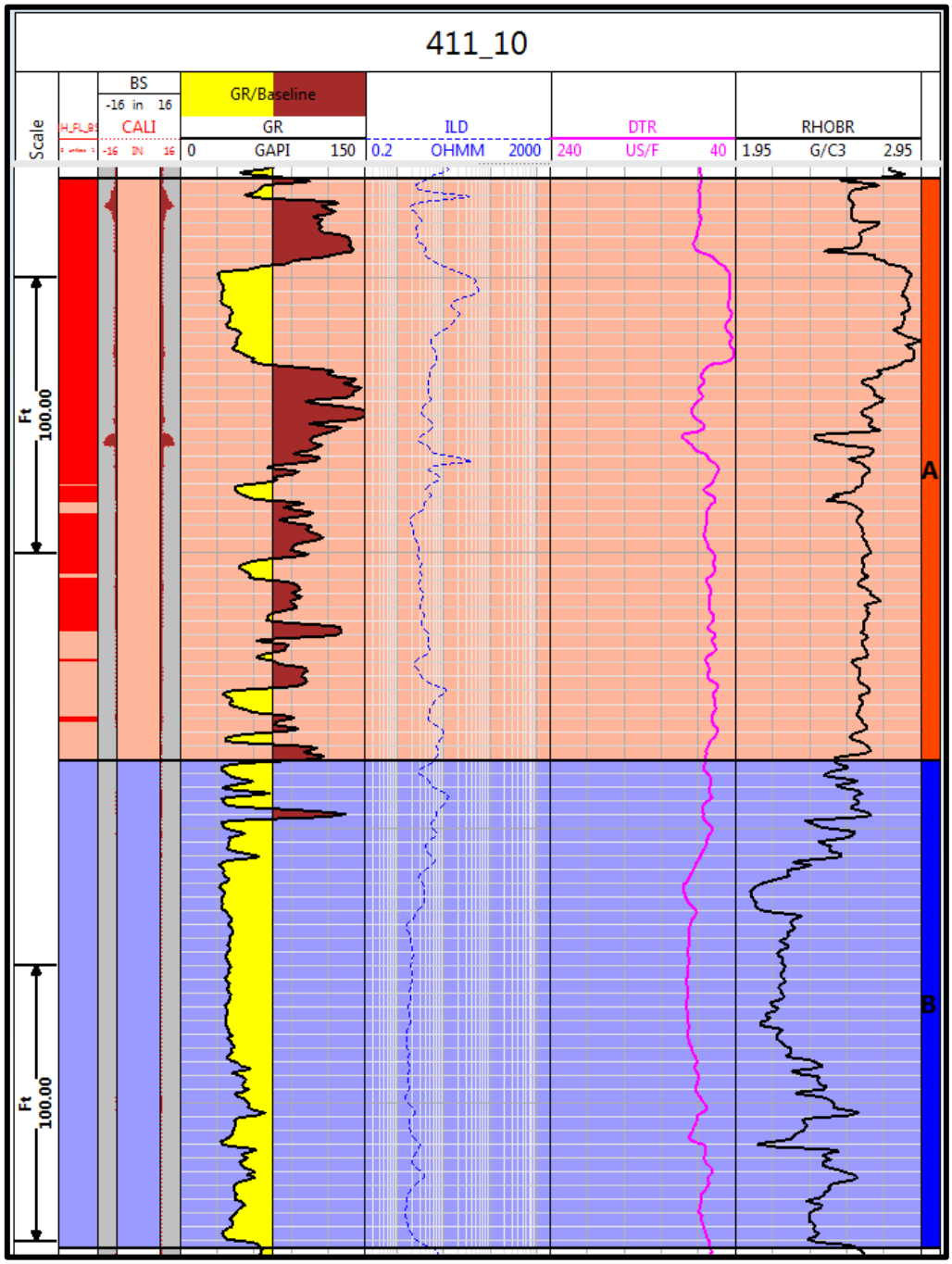

Figure 5. Logs for well 411_10.

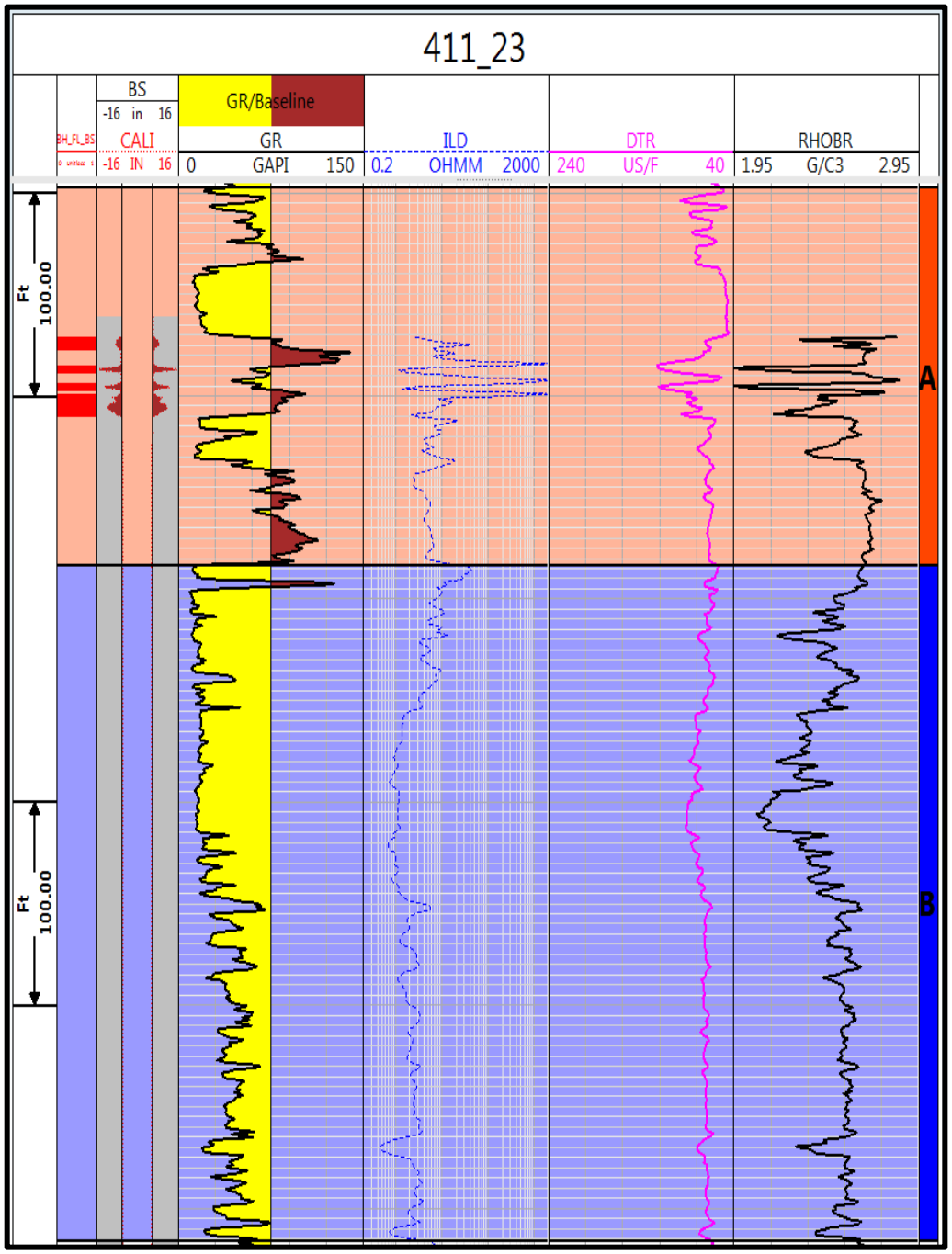

Figure 6. Logs for well 411_23.

CHAPTER 3

PETROPHYSICS ANALYSIS AND DATA CONDITION

3.1 Introduction

Petrophysics combines well logs, cores, mud-logs and other different data for evaluating, predicting and establishing the formation lithology, porosity, hydrocarbon saturation and permeability. Petrophysics is also used to estimate the economic feasibility of a well.

This chapter focuses on Geophysical Well Log Analysis (GWLA) and petrophysical methods for lithology, porosity and water saturation estimation using the available well logs data and briefly discusses the results.

3.2 Methodology

Well log analysis for geophysics differs from conventional log analysis in many aspects. In surface seismic usage, the vertical dimension of the zone of interest is always much larger than that of the hydrocarbon production zones. Geophysicists need elastic rock properties over the entire interval through which the seismic waves passed from the topographic surface to the total depth. This section of the thesis summarizes the methods used for quality control (QC) of logs, conditioning logs and estimating petrophysical properties.

3.2.1 Geophysical Well Log Analysis (GWLA)

Logs are affected by wellbore washout, casing points or mud filtrate invasion over different intervals. In some old wells, density, compressional or shear sonic logs are missed in a particular zone or are not measured at all. Therefore, elastic logs need to be corrected/predicted over the washout and missing intervals. This kind of analysis procedure is known as geophysical well log analysis (GWLA). The main goal of GWLA is preparing good quality data that can be used in quantitative seismic reservoir interpretation (Walls, 2004). GWLA consists of QC and data conditioning methods.

3.2.1.1 Quality Control

High quality log data is required within the reservoir and inter-well intervals. Therefore, the creation of histograms, and cross-plot and data plot data in depth assists in determining log data quality levels (Figure 7). The main goal of creating a histogram of logs (e.g., sonic, density and gamma ray) for multiple wells in the same field is to show consistency over different zones (Gunarto, 2010). Any observed inconsistency relates to the variations between the wells due to: differences in environmental conditions, borehole size, mud weight, mud type, missing intervals or using different tool from different service providers.

The differential caliper (DIFCAL), caliper log minus bit size, and density correction (DRHO) logs detect bad borehole conditions. For example, the density tool uses a pad of contact against the borehole wall and its measurement is severely affected by poor contact. Creating cross-plots of different well log data, including: compressional and shear velocities (V_p, V_s respectively) versus porosity, V_p versus V_s, acoustic impedance (I_p), (V_p multiplied by density) versus V_p/V_s, etc., color-coded by gamma ray, saturation or clay content all help to QC logs quality.

3.2.1.2 Well Log Conditioning

The sonic and density logs are affected in washout intervals. Therefore, the sonic waves are attenuated and a resulting cycle skip. This occurs where a wave signal of the first arrival dampens and shows a spike or abrupt change at a higher travel time (Rider, 1996). Cycle skips can be removed by different methods. First of these is the despike filter that applies median smoothing on the cycle skip flags to eliminate out-ranged values (Burch, 2002). The second method defines a relationship between any other wireline logs such as density, resistivity, gamma ray, etc. versus sonic slowness to generate a model for sonic data to replace cycle skip intervals.

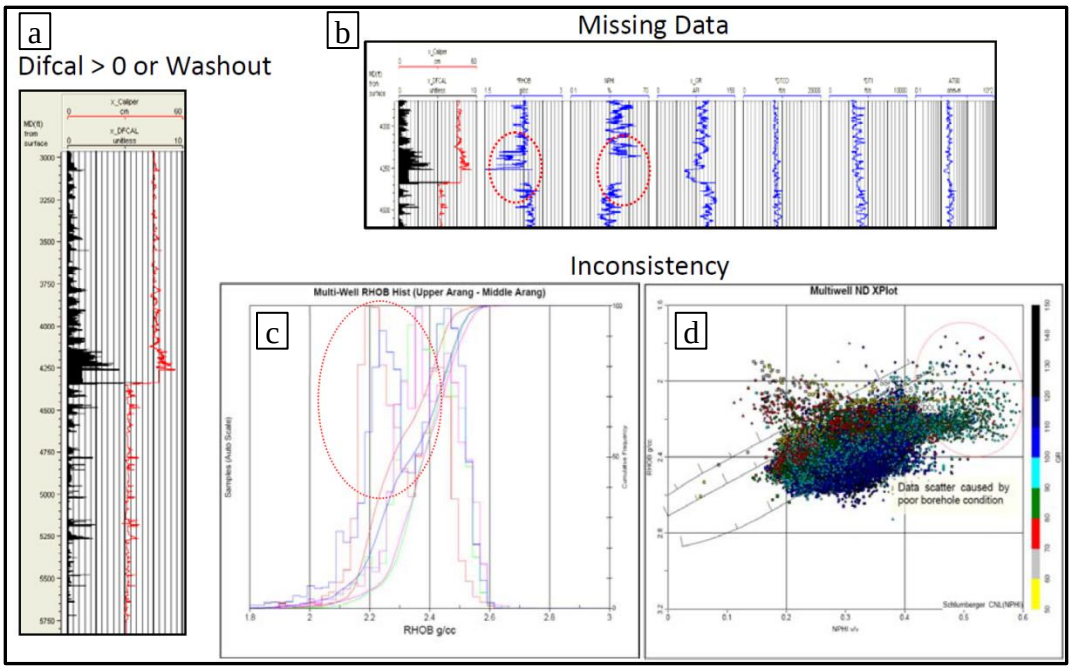

Figure 7. QC measured logs data tools: bad borehole condition, missing and data inconsistency. a) Caliper and differential caliper logs, b) Different logs in depth showing missing data, c) Histogram of density logs in multiple wells and d) Density vs. Neutron cross-plot color-coded by gamma ray (Gunarto, 2010).

Density tools read close to the borehole wall and should be in perfect contact with the wall. Therefore, their logs are affected severely by borehole conditions such as tool position and drilling mud. Generally, compressional velocity and bulk density have a robust relationship

(Gardner et al., 1974), so when velocity increases, density also increases (Figure 8). Gardner et al. (1974) established a set of relationships between bulk density and *P*-wave velocity (equation 3.1) for brine-saturated sedimentary rocks using laboratory measurements.

$$\rho_b = a\, V_p^c \qquad (3.1)$$

where:

ρ_b is the bulk density in *g/cc*, V_p is the *P*-wave velocity in *km/sec*, and *a*, *c* are constants.

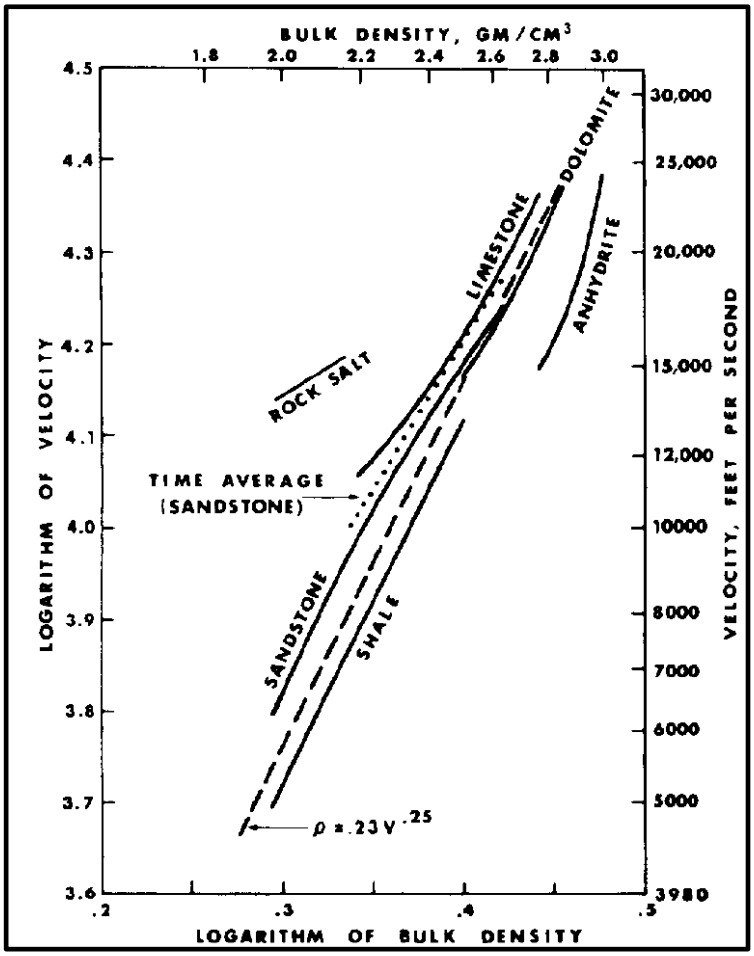

Figure 8. Velocity-Density relationships for different lithologies (Gardner et al., 1974).

In Gardner's equation, lithological variation is maintained by using different coefficients for each lithology type (Table 1).

Table 1. Coefficients for Gardner relations for different lithology (Castagna et al., 1993).

Lithology	*a*	*c*
Shale	1.75	0.265
Sandstone	1.66	0.261
Limestone	1.5	0.225
Dolomite	1.74	0.252
Anhydrite	2.19	0.160

3.2.2 Reservoir Properties

Elastic properties are controlled by several reservoir properties including porosity, lithology and saturation (Avseth et al., 2005). In this section of the thesis, I will only focus on the estimation of these three properties – methods that require generating the rock physics model.

3.2.2.1 Shale Volume

In the absence of any radioactive mineral in the formation, the gamma ray tool is essential to determine the presence of shale in the formation evaluation workflow (Rider, 1996).

The gamma ray shale index (I_{GR}) is defined as (equation 3.2).

$$I_{GR} = \frac{GR_{log} - GR_{clean}}{GR_{shale} - GR_{clean}} \qquad (3.2)$$

where:

GR_{log} is the measured gamma ray log response in the well, GR_{clean} is the log response in a shale free zone defined as "sand line or GR_{min}" and GR_{shale} is the log response in a shale zone defined as "shale line or GR_{max}".

Figure 9 displays sand and shale lines in gamma ray measurements. Some interpreters assume that volume of shale equals shale index, but this overestimates the shale volume (Rider, 1996). Therefore, to provide more reliable estimates of shale volume, empirical relations are developed for different geological ages and areas. Clavier et al., (1971) developed a relation to calculate the shale volume V_{sh},

$$V_{sh} = 1.7 - [3.38 - (I_{GR} + 0.7)^2]^{1/2} \qquad (3.3)$$

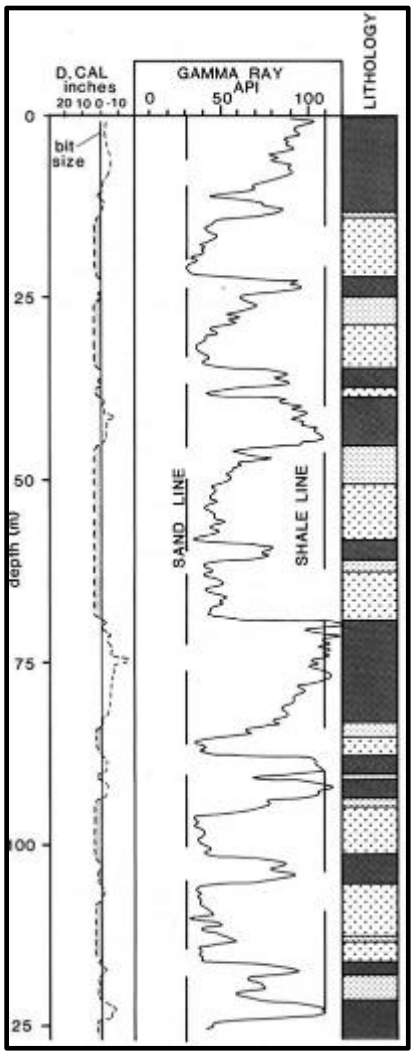

Figure 9. Sand and shale lines for shale volume calculation. Tracks from left: the first shows caliper and bit size logs; the second includes a gamma ray log, sand and shale lines; the third is lithology interpretation (Rider, 1996).

3.2.2.2 Porosity

Total porosity (ϕ_T) is the ratio of a pore volume within a rock to the total bulk volume of the rock (Rider, 1996), commonly expressed as a percentage (equation 3.4). Effective porosity (ϕ_E) is the ratio of the interconnected pore space to the total bulk volume.

$$\emptyset = \frac{Pore\ Volume}{Total\ Volume} \times 100 \qquad (3.4)$$

Porosity can be estimated from sonic log, density log, neutron log or combination between any two of them (Western Atlas, 1992).

The density tool is the most reliable porosity-sensitive device because its measurements are more sensitive to porosity than to lithology (Western Atlas, 1992). It is used to calculate porosity as:

$$\emptyset_T = \frac{\rho_{mat} - \rho_b}{\rho_{mat} - \rho_f} \qquad (3.5)$$

where:

ϕ_T is total porosity, ρ_b is bulk density, ρ_{mat} is matrix density and ρ_f is fluid density.

Matrix and fluid densities in many cases are selected based on the knowledge of the lithology and fluid type of the interest interval (Western Atlas, 1992). The common sedimentary rocks and fluids have the typical matrix density values listed in Table 2.

Table 2. Typical density values for different materials (Western Atlas, 1992).

Material	Density (g/cm^3)
Quartz	2.65
Calcite	2.71
Dolomite	2.87
Anhydrite	2.96
K-feldspar	2.56
Fresh water	1.00
Saltwater, 120,000 ppm NaCl	1.08
Oil (medium gravity)	0.80
Gas (160° F, 5000 psia)	0.20

The effective porosity determined by density log can be calculated as follows:

$$\emptyset_{T_{sh}} = \frac{\rho_{mat} - \rho_{sh}}{\rho_{mat} - \rho_f} \quad (3.6)$$

$$\emptyset_E = \emptyset_T - V_{sh} * \emptyset_{T_{sh}} \quad (3.7)$$

where: ϕ_{Tsh} is total shale porosity, ρ_{mat} is matrix density, ρ_{sh} is shale density, ρ_f is fluid density and V_{sh} is volume of shale.

3.2.2.3 Water Saturation

Water saturation (S_w) is the fraction of porosity in the reservoir rocks that is filled with water (Schlumberger, 1987). Determining water saturation is one of the most important objectives of a well log interpretation. There are many methods and equations to calculate water saturation. Archie's method is one of the well-known equations that is used to estimate water saturation based on resistivity measurements, as follows:

$$S_w^n = \frac{F\, R_w}{R_t} \quad (3.8)$$

where:

S_w is the water saturation, R_w is the formation water resistivity, R_t is the measured formation resistivity, n is the saturation exponent in most cases it equals to a default value of 2.0 and

F is the formation resistivity factor. F can be estimated from porosity as $F = a / \phi^m$, where a is a constant and m is the cementation exponent of the rock ranging between 1.8-3 (Rider, 1996).

3.2.2.4 Lithology Computation

The volume of various lithologies present in the well is calculated by equations that express different log responses to each mineral (Gardner, 1980). The Litho-Density log interpretation method, which is designed by Schlumberger to estimate up to four minerals, is used in this study to compute lithology volumes. The input logs for this method were: effective porosity, shale volume, flushed zone water saturation and bulk density.

3.3 Results and Discussion

The basic steps for any rock physical-petrophysical analysis is presented in Figure 10. I applied this workflow in this study using available logs and wells. This kind of workflow is an iterative process between the steps, which enhance the logs quality, and leads to reduce uncertainties of the rock physics model output.

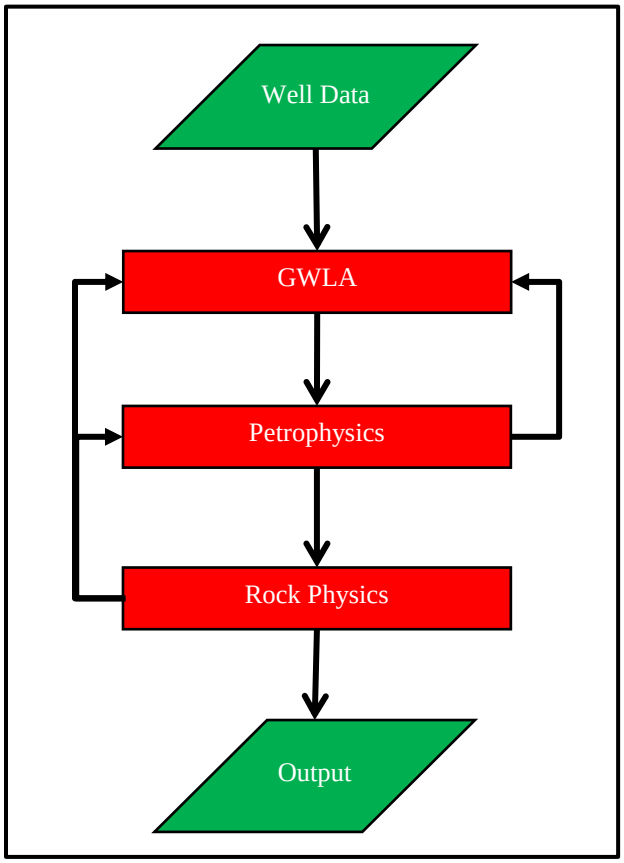

Figure 10. Rock physics – Petrophysics integrated workflow.

3.3.1 Geophysical Well Log Analysis

The workflow in Figure 11 presents the general steps of GWLA. The compressional velocity logs in this study were de-spiked in few depth intervals. In contrast, density logs were severely affected in the washout intervals, especially in zone-A. Well 411_10 showed

a better quality and was used to create a multi-linear regression (MLR) relation between different logs, to correct the density values in affected intervals (equation 3.9). In zone-B, the Gardner relation (equation 3.10) was used to correct the density values in the poor-condition intervals.

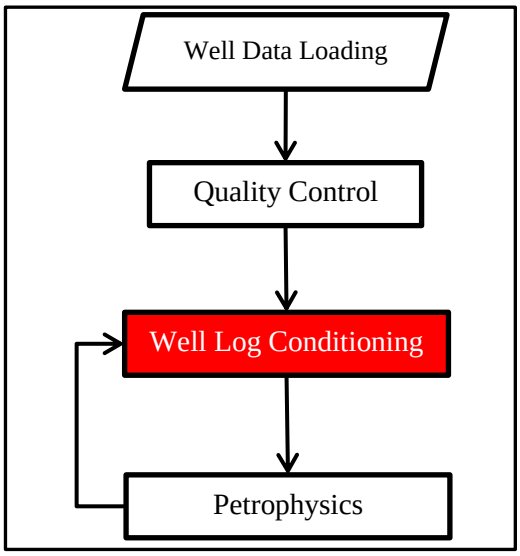

Figure 11. The general GWLA workflow.

$$\rho = a\ \ GR + b\ \ V_p + c \qquad (3.\ 9)$$

where:

ρ is density, GR is gamma ray, V_p is compressional velocity, a = 0.001, b = 0.118 and c = 2.036. The Gardner (power) relation is given as:

$$\rho = a\ V_p\, b \qquad (3.\ 10)$$

where:

ρ is density, V_p is compressional velocity, a = 1.27 and b = 0.46.

The MLR relation used on zone-A increased the consistency and quality of the density data as presented in Figure 12. The Gardner (power) relation used in zone-B also improved the densities quality Figure 13.

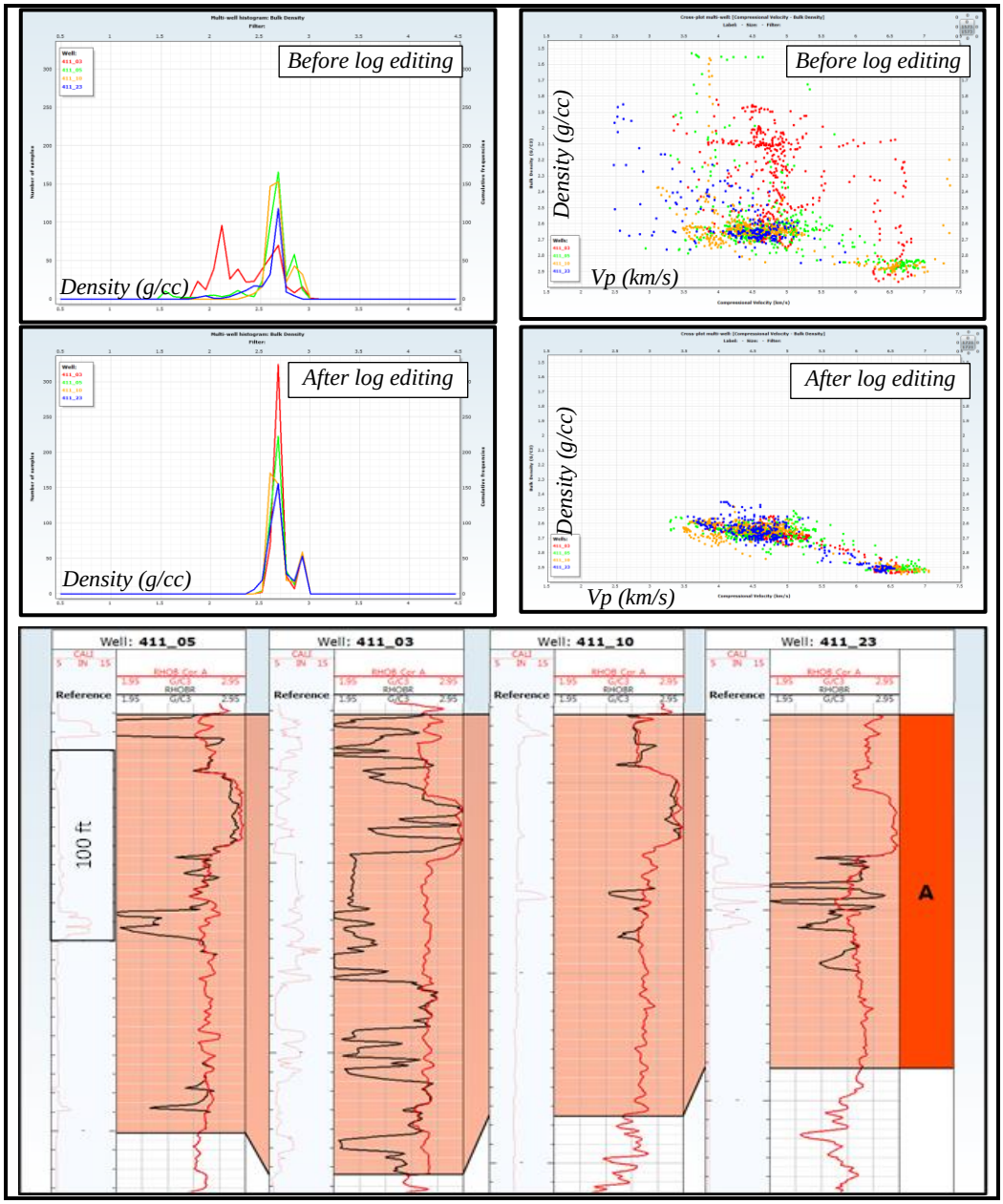

Figure 12. QC density logs before/after editing in the zone-A. The top row of the figure, left, shows density histogram for each well and the right is density vs. V_p cross-plot before correction. The second row, left, shows density histogram for each well and the right is density vs. V_p cross-plot after correction. The third row shows measured density logs in each well (black curves) and conditioned densities (red curves). Note: tops aligned to the zone-A top.

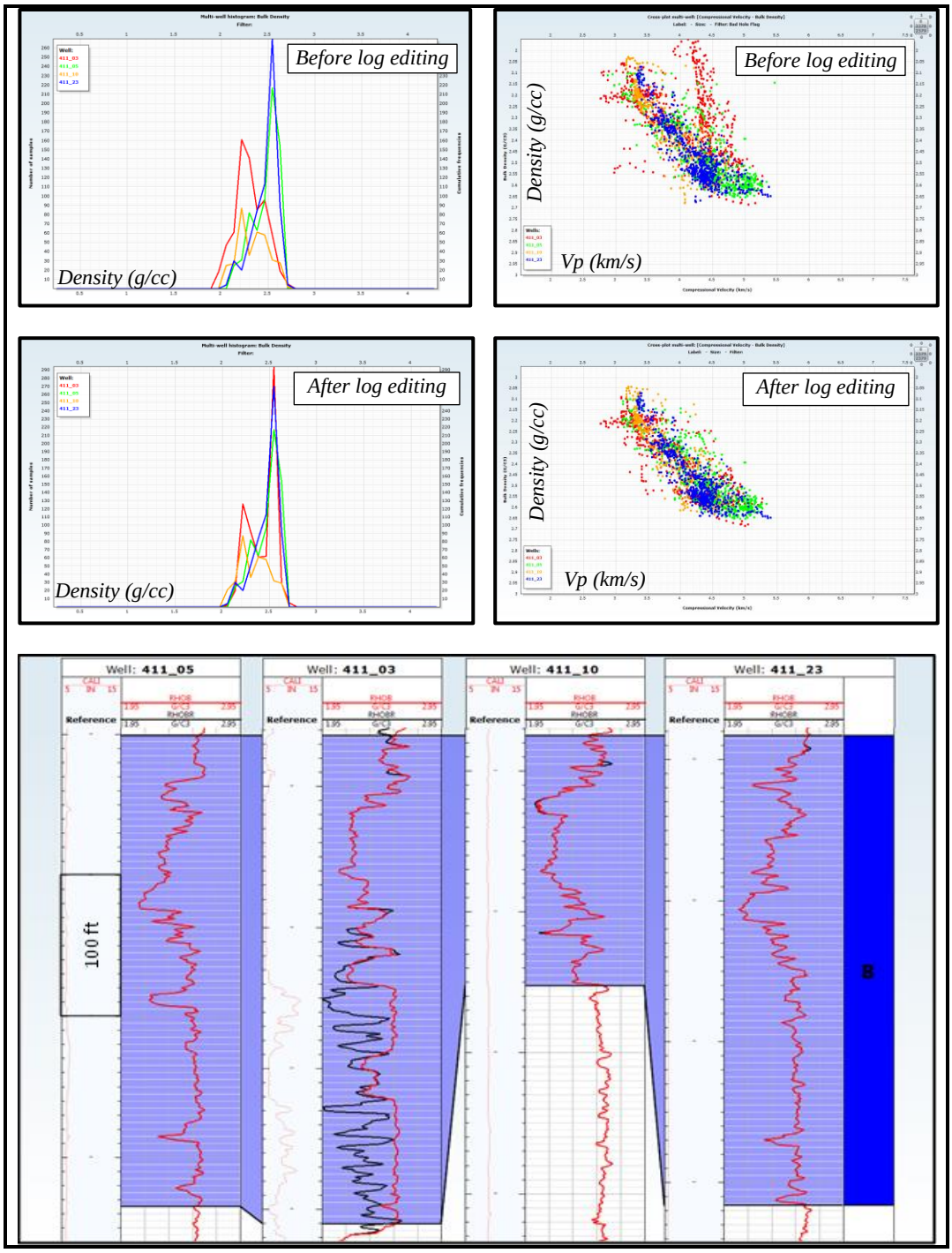

Figure 13. QC density logs before/after editing in the zone-B. Figures as described in previous figure. Note: tops aligned to the zone-B top.

3.3.2 Reservoir Properties

Some of the reservoir properties (e.g., porosity) can be calculated using elastic logs. Therefore, logs conditioning is very important to improve the logs quality that contribute to enhance the petrophysical properties results. Other petrophysical properties (e.g., volume of shale and water saturation) can be calculated using gamma ray and resistivity logs. Therefore, in both zones (A and B) I used gamma ray logs to calculate shale volume. Different sand and shale lines were selected on the gamma ray histograms as displayed in Figure 14, where the red and magenta vertical lines are the minimum and the maximum gamma ray values on zone-A with corresponding blue and gray lines for zone-B. The Clavier et al. (1971) equation is used to calculate the volume of shale in the study zones. The results of this calculation show low amounts of shale in the reservoir, zone-B, compared to the overlying carbonate layer, zone-A (Figure 15).

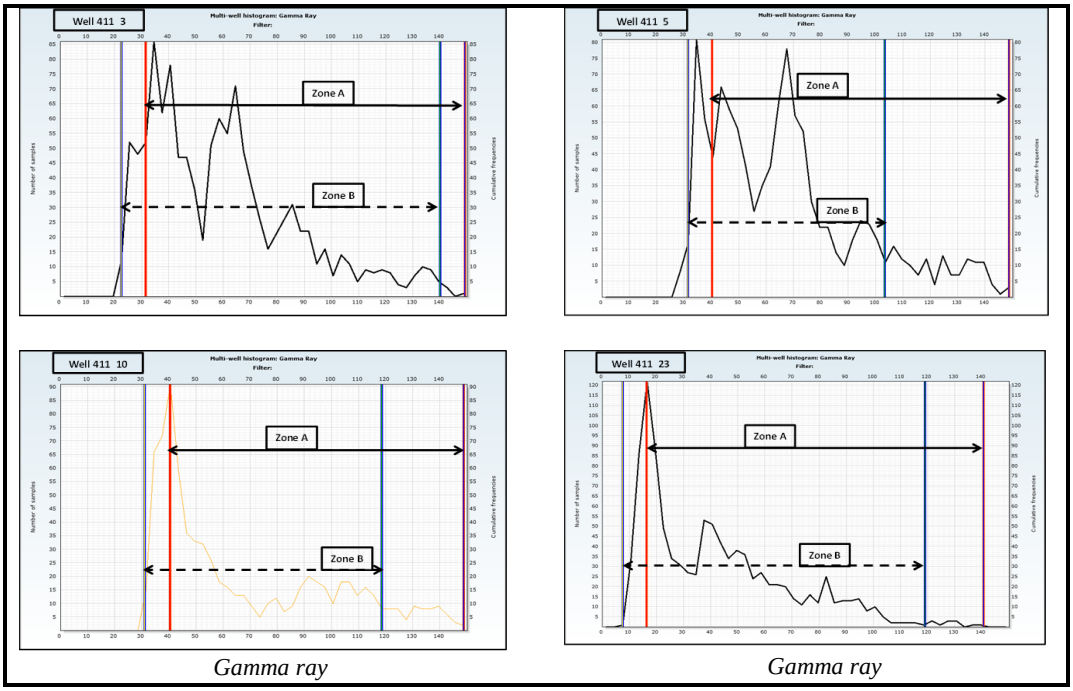

Figure 14. Selected sand and shale lines for each well in both zones.

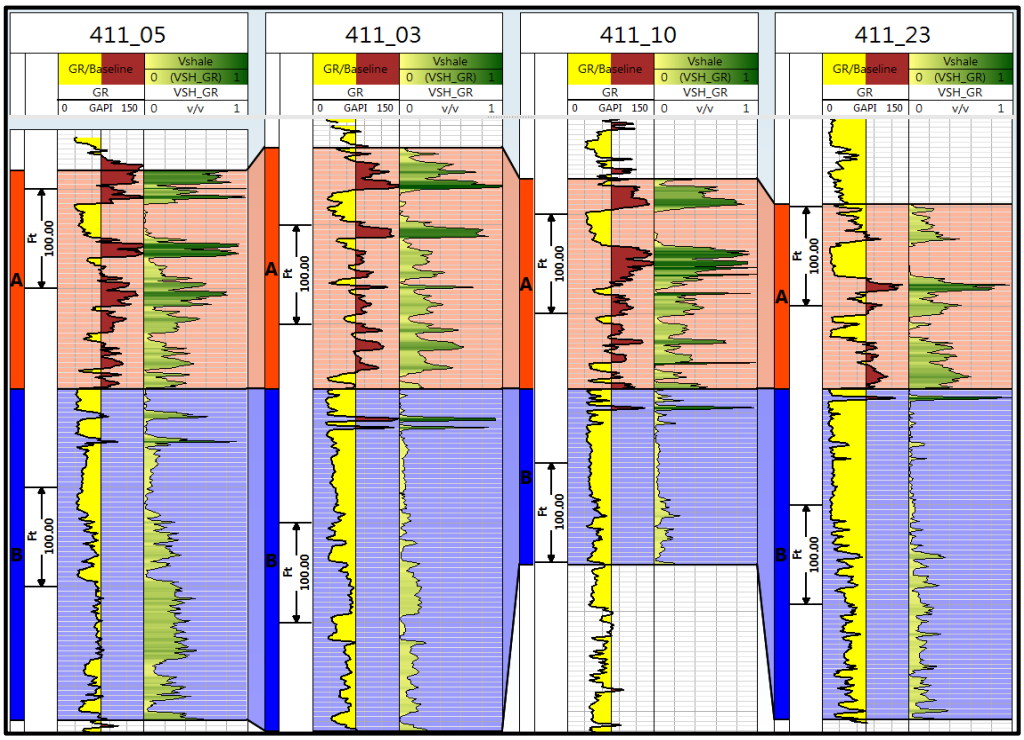

Figure 15. Shale volume for each well. Tracks form left to right: zone names, depth, gamma ray and shale volume.

Density logs were used to estimate porosity in both zones. In zone-A, the average bulk densities were assumed to be 2.7 g/cc and 2.6 g/cc for matrix and shale, respectively. Whereas in zone-B, 2.62 g/cc and 2.48 g/cc were used as the average bulk densities for matrix and shale, respectively. In the reservoir or zone-B, fluid density assumed to be 0.8 g/cc and 1.0 g/cc in zone-A. These assumptions were made based on the average density logs responses in both zones. The estimated total and effective porosities for each well are displayed in Figure 16. The results show that the average porosity is around 20% in the good quality interval within reservoir. The total and effective porosities are almost the same due to the low amount of shale, especially in the reservoir.

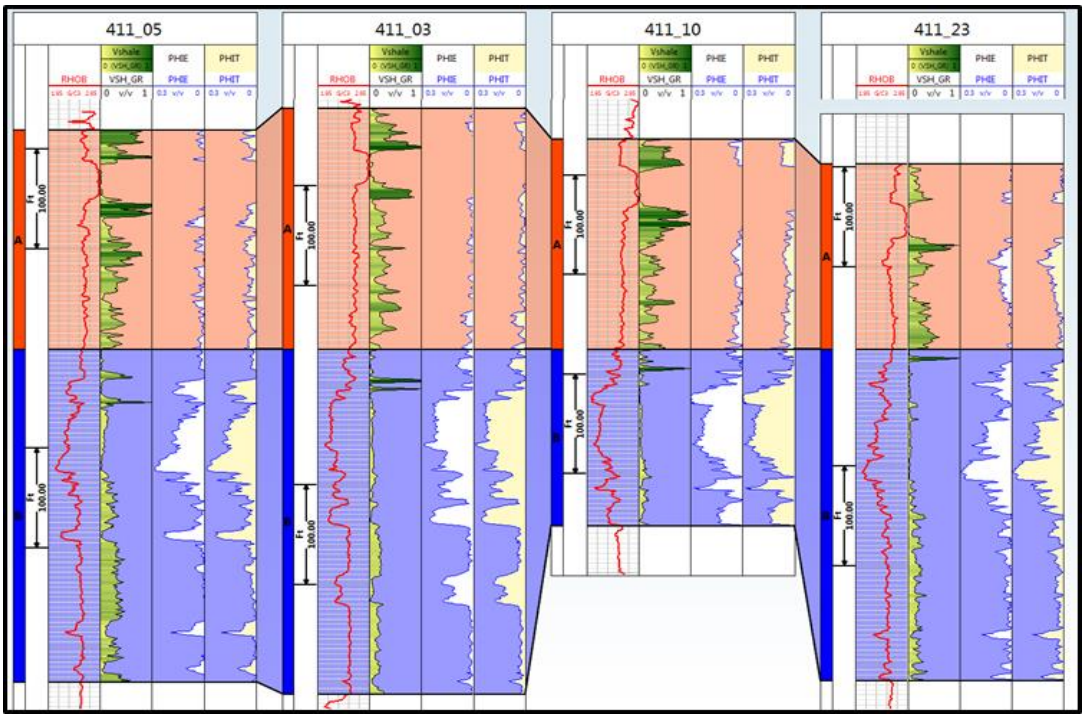

Figure 16. Porosity estimated from density logs. Track from left to right for each well: zone name, depth, density, shale volume, effective and total porosity. Note: tops aligned to the zone-B top.

Archie's equation was used to estimate water saturation. The Archie's parameters *a*, *m* and *n* used for zone-A and zone-B are listed in Table 3. The saturation results for all wells are presented in Figure 17. Zone-A is almost fully water-saturated whereas the saturation varies in zone-B. The lower part of the reservoir is most likely water-saturated and the upper part varies between water- and hydrocarbon-saturated in all wells. The middle interval of the reservoir shows less water saturation over all wells.

Table 3. Archie's parameters for the study area

Zone name	*a*	*m*	*n*
Zone-A	1	2	2
Zone-B	1	1.97	1.7

The Litho-Density interpretation method is applied to compute lithology volumes. In zone-A, three minerals, dolomite, limestone and anhydrate plus shale are used to determine

lithology volume, while in zone-B, quartz and shale were assumed to be the only minerals in the reservoir. The lithology computation results for each well are presented in Figure 18.

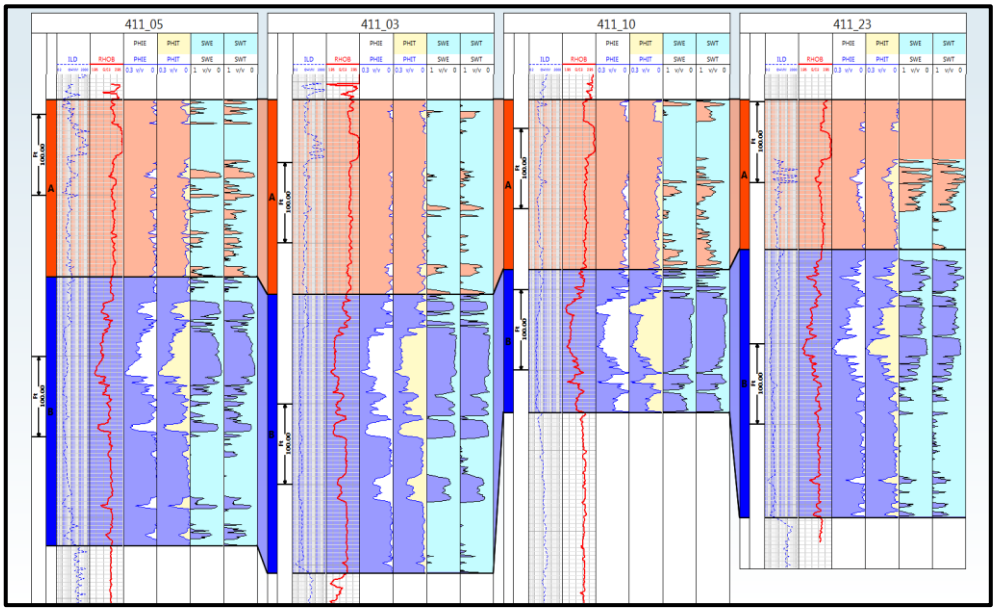

Figure 17. Estimated water saturation for each well. Tracks from left to right: zone name, depth, deep resistivity, density, effective porosity, total porosity, effective and total water saturation. Note: tops aligned to Zone-A top.

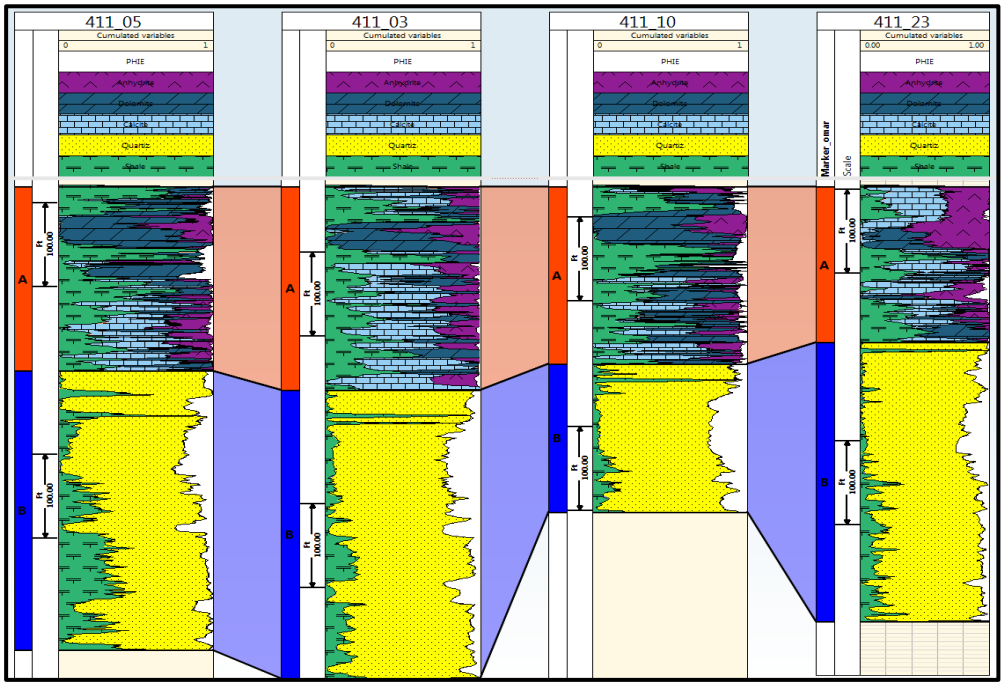

Figure 18. Lithology volumes results for each well. Tracks from left to right: zone names, depth and lithology volume. Note: tops aligned to zone-A top.

CHAPTER 4

ROCK PHYSICS MODELING

4.1 Introduction

Generally, seismic properties — density, compressional- and shear-wave velocities — are controlled by many factors, such as lithology (composition and texture), porosity, pore fluids type, differential pressure, temperature, wave frequency, anisotropy, etc. These factors interconnect in a way that could change seismic properties. Therefore, understanding the relations between these factors and seismic elastic properties is key to creating accurate rock physics models. Table 4 lists factors that affect seismic properties in sedimentary rocks, with increasing importance from top to bottom (Wang, 2001).

Table 4. Rock, fluid and environmental properties governing elastic properties in sedimentary rocks (Wang, 2001)

Importance ↓	Rock Property	Fluid Property	Environmental Property
	Compaction	Viscosity	Frequency
	Consolidation history	Density	Stress history
	Age	Wettability	Depositional environment
	Cementation	Fluid composition	Temperature
	Texture	Phase	Reservoir process
	Bulk density	Fluid type	Production history
	Clay content	Gas-oil, gas-water ratio	Layer geometry
	Anisotropy	Saturation	Net reservoir pressure
	Fractures		
	Porosity		
	Lithology		
	Pore shape		

The velocity-porosity relation is a key method to connect reservoir properties to elastic properties. In consolidated and unconsolidated formations, the V_p-ϕ relations have different trends. Figure 19a shows an enhanced version of the critical porosity model (Nur, 1998), which is a linear interpolation between bulk modulus (K) and shear modulus (μ) between porosities, $\phi = 0$ and $\phi = \phi_c = 38\%$ for sandstone. The rock critical porosity, ϕ_c, separates the load-bearing sediments at porosity $\phi < \phi_c$ and suspensions at porosity $\phi > \phi_c$ (Mavko et al., 2009). Figure 19b shows the V_p- and V_s-wave velocities versus porosity, which can be used easily to separate the consolidated and unconsolidated rocks at ϕ_c. The consolidated and unconsolidated trends in both elastic moduli and velocity versus porosity relations are typical of grain-supported sandstones. Generally, in consolidated sands the major factors accountable for velocity variation are porosity and clay content. In contrast, in unconsolidated sands grain sorting, loading history and cementation ratio take a role in velocity variation (Vernik, 1997). Several authors have established important relationships between the elastic properties and reservoir parameters such as porosity and clay content (e.g., Han, 1986), diagenesis (e.g., Dvorkin and Nur, 1996), lithology (e.g., Greenberg and Castagna, 1992), as well as pore fluids (e.g., Wang et al., 1990; Batzle and Wang, 1992). The above relations and others published contribute to assist in selecting an appropriate rock physics model.

Rock physical models are classified into three general classes: theoretical, empirical and heuristic (Avseth et al., 2005).

1- Theoretical methods yield mathematical expressions of the elastic properties of rock but assumptions must be made to simplify the mathematics. Sometimes, these assumptions are over-simplified and even unrealistic (Wang, 2000). Elastic theoretical models include:

- **Inclusion models** that deal with the rock as an elastic solid containing cavities (inclusions) representing the pore space. Common inclusion models assume that the pores are idealized ellipsoidal or penny-shaped cavities (e.g., Kuster and Toksoz, 1974).

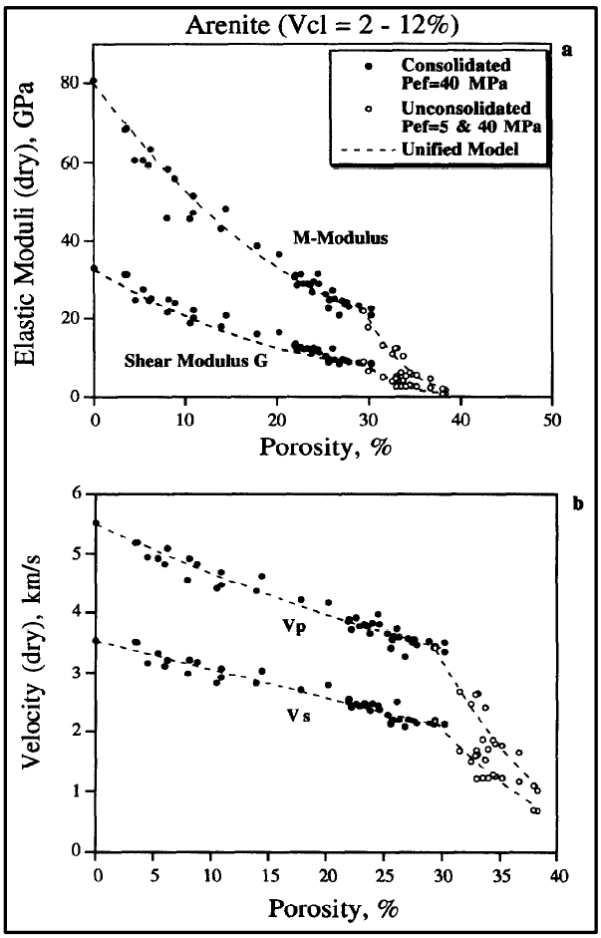

Figure 19. a) Dry frame elastic moduli vs. porosity and b) dry velocities vs. porosity, for clean consolidated and unconsolidated sandstones. Models shows abrupt change point at porosity of 30%, (Vernik, 1997).

- Contact models determine the elastic properties of granular media by shape changes and stiffness of grain contacts. Most of the contact models are based on the Hertz-Mindlin (Mindlin, 1949) model of the normal and shear contact stiffness of two particles in contact.

- Computational models estimate the actual grain-pore microgeometry using different measurement methods, such as thin section or CT-scan imaging. These models do not rely on pore geometry and they have the ability to quantify elastic features observed in thin sections.

- **Bound models** describe how the effective elastic moduli of a mixture of grains and pores are calculated by knowing the volume fractions of different phases, the elastic moduli of the various phases, and the geometric details of how the phases are arranged relative to each other (Mavko et al., 2009). The concept of the upper and lower bounds on the elastic bulk and shear moduli for a simple mixture of a mineral and fluid is presented in Figure 20.

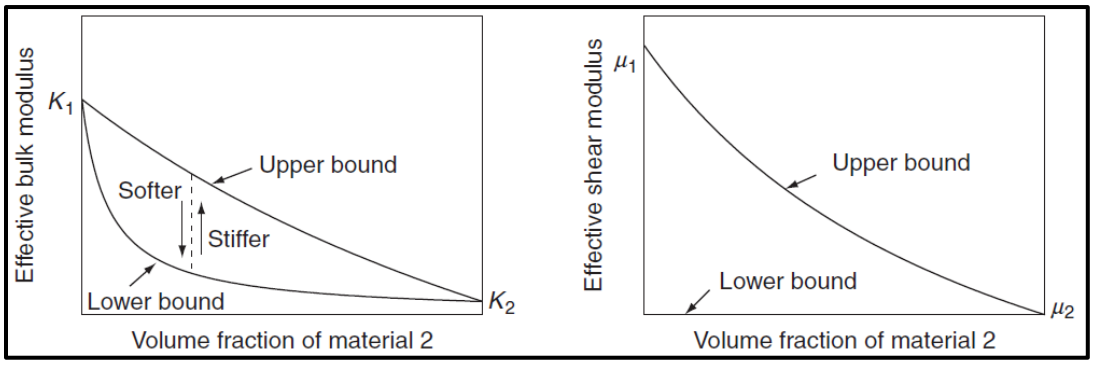

Figure 20. The upper and lower bounds concept on the elastic bulk and shear moduli (Mavko et al., 2009).

- **Transformation models** are free of geometric assumptions. One of the most widely used transformation models is Gassmann's model (Gassmann, 1951). Gassmann derived an equation to calculate the bulk modulus of a fluid-saturated porous medium using the known bulk moduli of the matrix, the frame (dry) and the pore fluid.

2- Empirical models generally provide simple mathematical formulations and determine coefficients by calibrating a regression to observed data. There are several well-known empirical models such as Han's linear regression (Han, 1986), where he determined velocities using porosity and clay content. Greenberg and Castagna (1992) used empirical polynomial relations to estimate shear velocity from compressional velocity, brine saturated rocks and lithology. Gardner et al. (1974) suggested a useful empirical relation between compressional wave velocity and density.

3- Heuristic models are sometimes defined as pseudo-theoretical models (e.g., Wyllie et al., 1958, time average equation) in clean, consolidated water-saturated rocks.

4.2 Theoretical Background

The basics of elasticity followed by shear velocity prediction techniques and the concept of bounds on elastic properties will be briefly discussed in this section of the thesis. Then Gassmann's fluid substitution equation and its assumptions will be used to explain these concepts. Finally, the velocity-porosity behavior of clastic rocks using contact models will be described.

4.2.1 Seismic Waves

In homogenous, isotropic and elastic media, seismic velocity is expressed generally by elastic constants and density (equation 4.1). This equation can be rearrange depending upon the wave type and the elastic constants. There are two body waves for an elastic isotopic medium. The first wave type is compressional (equation 4.2) and the second is shear (equation 4.3) (Bakhorji, 2010), with the velocity for each type being expressed by the following equations.

$$Velocity = \sqrt{\frac{Elastic\ constants}{Bulk\ Density}} \quad (4.1)$$

$$Compressional\ Velocity\ (V_p) = \sqrt{\frac{Bulk\ modulus\ (K) + 4/3\ Rigidity\ (\mu)}{Bulk\ Density\ (\rho)}} \quad \text{or}$$

$$Compressional\ Velocity\ (V_p) = \sqrt{\frac{Compressional\ modulus\ (M)}{Bulk\ Density\ (\rho)}} \quad (4.2)$$

$$Shear\ Velocity\ (V_s) = \sqrt{\frac{Rigidity\ (\mu)}{Bulk\ Density\ (\rho)}} \quad (4.3)$$

Other elastic constants, such as Poisson's ratio (*PR*) (equation 4.4), Lamé's (λ) coefficient (equation 4.5) and Young's (*E*) modulus (equation 4.6) can be derived from V_p, V_s and density.

$$PR = \frac{1}{2}\frac{V_p^2/V_s^2 - 2}{V_p^2/V_s^2 - 1} \quad (4.4)$$

$$\lambda = \rho\,(V_p^2 - 2V_s^2) \quad (4.5)$$

$$E = \frac{\rho V_s^2\,(3\,V_p^2 - 4\,V_s^2)}{V_p^2 - V_s^2} \quad (4.6)$$

4.2.2 Shear Velocity Prediction

Greenberg and Castagna (1992) developed a general method to predict shear wave velocity using compressional wave velocity in fully water-saturated porous rocks. The method assumed the shear wave velocity could be estimated by averaging the harmonic and arithmetic means of the pure constituents' porous-lithology and compressional velocities (equation 4.7):

$$V_s = \frac{1}{2}\left\{\left(\sum_{i=0}^{L} X_i \sum_{j=0}^{N_i} a_{ij}\, V_p^{\,j}\right) + \left(\frac{1}{\frac{\sum_{i=0}^{L} X_i}{\sum_{j=0}^{N_i} a_{ij}\, v_p^{\,j}}}\right)\right\}; \quad \sum_{i=0}^{L} X_i = 1 \quad (4.7)$$

where:

V_p and V_s are the compressional and shear wave velocities, respectively, of the composite rock. L is the number of pure mono-mineral porous constituents. X_i is the dry lithology volume fraction of lithological constituent i. a_{ij} are the empirical coefficients defined in Table 5 and $0 \leq N_i$ is the order of polynomial i.

Table 5. V_p-V_s regression coefficients for various lithologies (Greenberg et al., 1992).

Lithology	a_{i2}	a_{i1}	a_{i0}
Limestone	-0.05508	1.01677	-1.03049
Dolomite	-	0.58321	-0.07775
Sandstone	-	0.80416	-0.85588
Shale	-	0.76969	-.086735

Raymer et al. (1980) developed a model to estimate V_p in porous brine-filled rocks from porosity, solid and fluid P-wave velocities, respectively:

$$V_P = (1 - \emptyset)^2 V_{Ps} + \emptyset V_{Pf} \qquad (4.8)$$

Later, Dvorkin (2008) used Raymer's model and estimated shear wave velocity for porous multi-mineral rocks:

$$V_S = (1 - \emptyset)^2 V_{ss} \sqrt{\frac{(1-\emptyset)\rho_S}{(1-\emptyset)\rho_s + \emptyset \rho_f}} \qquad (4.9)$$

where:

V_{ss} is the shear-wave velocity of solid phase. ρ_s, ρ_f are solid and fluid densities, respectively.

4.2.3 Elastic Bounds

The simplest effective medium bounds models are Voigt (Voigt, 1910) and Reuss (Reuss, 1929) bounds. The Voigt upper bound is the arithmetic average of the elastic moduli of

individual components of a composite (equation 4.10). The Voigt bound assumes that the strain is uniform throughout the aggregate and gives the ratio of average stress to average strain, so that it is called an isostrain average (Figure 21a). The Reuss lower bound is the harmonic average of the elastic moduli of individual components of a composite (equation 4.11). The Reuss bound assumes that the stress is uniform throughout the aggregate and gives the ratio of average stress to average strain, so it is called an isostress average (Figure 21b). The average effective moduli of the two bounds can be calculated using Viogt-Reuss-Hill (VRH) average (equation 4.12) (Mavko et al., 2009).

$$M_v = \sum_{i=0}^{N} f_i M_i \qquad (4.10)$$

$$\frac{1}{M_R} = \sum_{i=0}^{N} \frac{f_i}{M_i} \qquad (4.11)$$

$$M_{VRH} = \frac{1}{2}(M_V + M_R) \qquad (4.12)$$

where: M is the elastic modulus of the aggregate formed by N materials, f_i is the volume fraction of the ith material and M_i is the elastic modulus of the ith constituent.

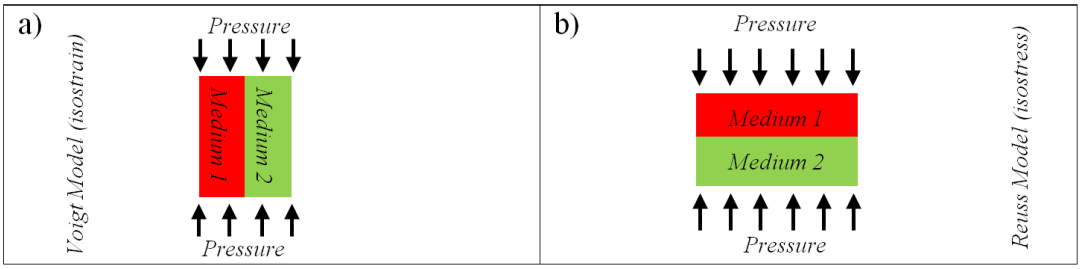

Figure 21. Graphical illustration of a) Voigt (isostrain) and b) Reuss (isostress) models for a two-component effective medium (Lakes, 2002).

The wide gap between the Voigt and Reuss bounds often makes the models of little practical use. Therefore, Hashin and Shtrikman, (1963) derived upper and lower bounds for the elastic moduli of multiphase materials, which represent the better and tighter bounds

for an isotropic elastic mixture than Voigt-Reuss bounds. For a mixture of two constituents, the Hashin and Shtrikman bounds are:

$$K^{HS\pm} = K_1 + \frac{f_2}{(K_2 - K_1)^{-1} + f_1\left(K_1 + \frac{4\mu_1}{3}\right)^{-1}} \quad (4.13)$$

$$\mu^{HS\pm} = \mu_1 + \frac{f_2}{(\mu_2 - \mu_1)^{-1} + 2f_1(K_1 + 2\mu_1)/\left[5\mu_1\left(K_1 + \frac{4\mu_1}{3}\right)\right]} \quad (4.14)$$

where: K^{HS+} and μ^{HS+}, upper bounds for the effective bulk and shear modulus, respectively, while K^{HS-} and μ^{HS-} are the lower bounds.

Generally, estimating upper and lower bounds is mainly based on material stiffness and softness. The upper bound term indicates that material is stiff and parameters in the (equations 4.13 and 4.14) would be subscripted with 1. If the materials were soft, the bound would be lower and the parameters would be subscripted with 1.

The physical explanation of the Hashin-Shtrikman bounds for any material bulk modulus is shown in Figure 22. The internal spheres (core) are filled by an assembly material 2 and are surrounded by spherical shells filled by material 1. Both cores and shell spheres have precise volume fractions f_1 and f_2, respectively. The upper bound is formed when the shell spheres are occupied by stiffer materials and the lower bound is formed when the cores spheres are filled by stiffer materials.

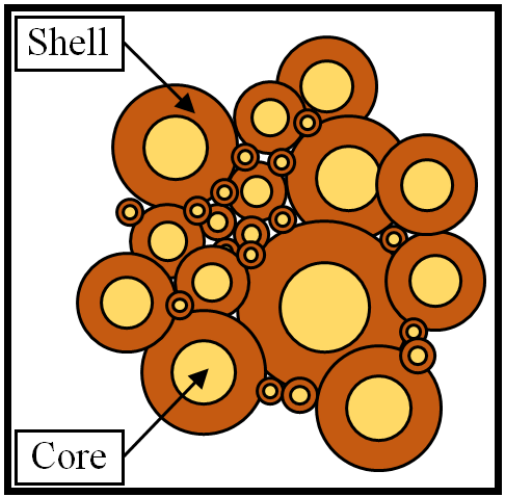

Figure 22. Physical explanation of the Hashin-Shtrikman bounds for bulk modulus of two-phase materials (Avseth et al., 2005).

Nur et al. (1998) introduced a description of critical porosity (ϕ_c) that provides more realistic upper bound for minerals. This critical porosity was described briefly in section 4.1 and the general physical concept is presented in Figure 23. The critical porosity values vary for rocks, where ϕ_c for sandstone is around 40% and for cracked igneous rock it is around 5%.

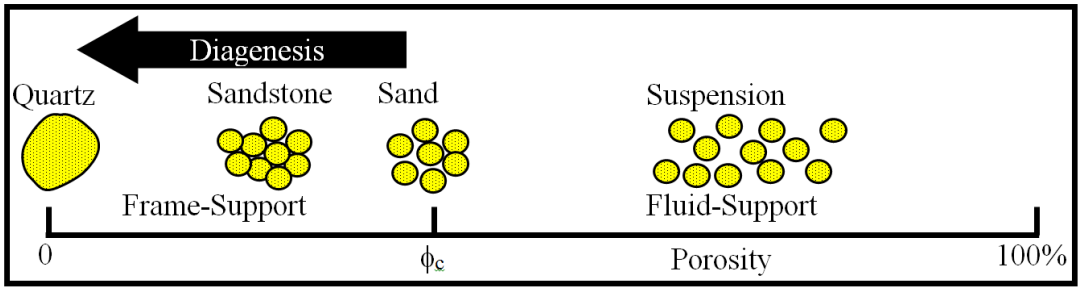

Figure 23. Physical meaning of critical porosity (Nur et al., 1998).

Nur et al. (1998) modified upper bounds by replacing the soft end member at 100% porosity with the suspension end member at critical porosity. In addition, he calculated the bulk modulus of the suspension less than critical porosity ($\phi<\phi_c$) using solid and soft bulk moduli by the Reuss average (equation 4.15). Then, he interpolated between the moduli of

solid point at porosity equal to zero and the suspension moduli at critical porosity (Nur el al., 1998).

$$K_c = \left[\frac{(1-\emptyset_c)}{K_s} + \frac{\emptyset_c}{K_{fl}}\right]^{-1} \quad (4.15)$$

$$K_{eff} = \left(1 - \frac{\emptyset}{\emptyset_c}\right) K_s + \frac{\emptyset}{\emptyset_c} K_c \quad (4.16)$$

$$\mu_{eff} = \left(1 - \frac{\emptyset}{\emptyset_c}\right) \mu_s \quad (4.17)$$

where: K_c is the bulk modulus at critical porosity; K_s, K_{fl} are solid and fluid bulk moduli, respectively. ϕ is porosity; ϕ_c is critical porosity; K_{eff}, μ_{eff} are effective bulk and shear moduli, respectively, and μ_s is the solid shear modulus.

4.2.4 Fluid Substitution

One of the most widely used models to substitute fluids is Gassmann's model (Gassmann, 1951). Gassmann derived equations to calculate the bulk modulus of a fluid-saturated porous medium using the known bulk moduli of the solid matrix, the frame (dry), the pore fluid and porosity. Equation 4.18 is one of the standard forms of Gassmann equation (Mavko et al., 2009):

$$\frac{K_{sat}}{K_s - K_{sat}} = \frac{K_{dry}}{K_s - K_{dry}} + \frac{K_{fl}}{\phi(K_s - K_{fl})} \quad (4.18)$$

where:

K_{sat} is the bulk modulus of the rock saturated with a fluid of bulk modulus K_{fl}. K_{dry} is the frame (dry) bulk modulus. K_s is the solid bulk modulus, and ϕ is the porosity.

Gassmann's model assumes that the fluid has no resistance to shear deformation; therefore, the effective shear moduli of the saturated (μ_{sat}) and dry rock (μ_{dry}) are equal:

$$\mu_{sat} = \mu_{dry} \quad (4.19)$$

The basic assumptions in the Gassmann's equation are (Avseth et al., 2005):

① The rock or porous medium (both the matrix and the frame) is macroscopically homogeneous.

② All pores are interconnected.

③ The pores are filled with a frictionless fluid (liquid or gas).

④ The solid-fluid system under study is closed (un-drained).

⑤ The relative motion between the fluid and solid is small and negligible compared to the motion of the saturated rock itself when the rock is excited by a wave.

⑥ The pore fluid does not interact with the solid in a way that would change the shear rigidity of the frame (softening or hardening).

4.2.5 Contact Theory

Mavko et al. (2009) described how the effective elastic properties of packing of spherical particles depend on normal and tangential contact stiffnesses of the two-particles combination (Figure 24). The normal stiffness (S_n) of two identical spheres is defined as the ratio of a confining force increment to the shortening of a sphere radius (equation 4.20). The tangential stiffness (S_t) of two identical spheres is the ratio of a tangential force increment to the increment of the tangential displacement of the center, relative to the contact region (equation 4.20).

$$\left.\begin{aligned} S_n &= \frac{\partial F}{\partial \delta} \\ S_t &= \frac{\partial T}{\partial \tau} \end{aligned}\right\} \qquad (4.\ 20)$$

where: S_n and S_t are the normal and the tangential stiffnesses, respectively. F is the normal force; T is the tangential force; δ is the normal displacement and τ is the tangential displacement.

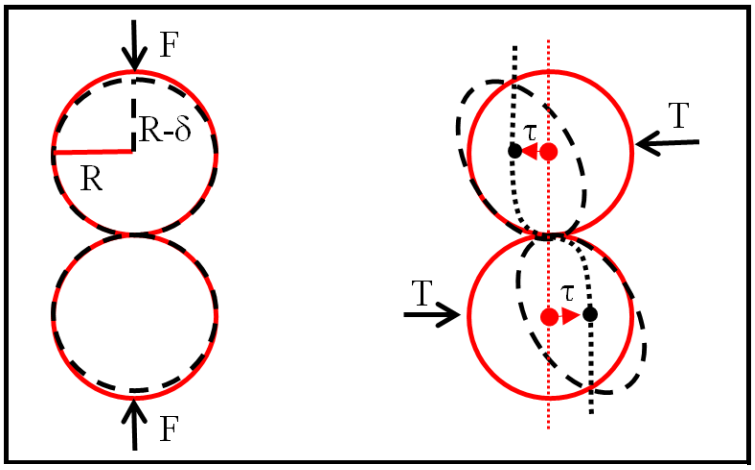

Figure 24. Normal and tangential displacement in a two-spherical particles system. *R* is the sphere radius (Mavko et al., 2009).

The effective bulk and shear moduli for a random sphere packing can be expressed by porosity, coordination number (the average number of contacts per grain), the sphere radius, and the normal and tangential stiffnesses of the two-sphere particles combination (Mavko et al., 2009).

$$K_{eff} = \frac{c\,(1-\emptyset)}{12\,\pi\,R}\,S_n \qquad (4.21)$$

$$\mu_{eff} = \frac{c\,(1-\emptyset)}{20\,\pi\,R}\,(S_n + 1.5\,S_t) \qquad (4.22)$$

where: K_{eff} and μ_{eff} are the effective bulk and shear moduli, respectively. R is the sphere radius and ϕ is porosity. S_n and S_t are the normal and tangential stiffnesses, respectively, and c is the coordination number.

Hertz-Mindlin Contact Theory

The elastic moduli of the dry well-sorted end-point at a critical porosity can be estimated by Hertz-Mindlin model (Mindlin, 1949). If the two identical spheres in this model are normally compressed, the radius of the contact area and the normal displacement is calculated as:

$$a = \left[\frac{3FR}{8\mu}\ (1 - PR)\right]^{\frac{1}{3}}; \qquad \delta = \frac{a^2}{R};$$

where:

μ is the shear modulus and *PR* is Poisson's ratio of the grain material.

If an effective pressure is applied to a random packing of identical spheres, the confining force between two particles can be calculated as (Mavko et al., 2009):

$$F = \frac{4\ \pi\ R^2 P}{c\ (1 - \emptyset)}\ ;\ a = R\ \left[\frac{3\pi\ (1 - PR)P}{2c\ (1 - \emptyset)\mu}\right]^{\frac{1}{3}}$$

where the effective pressure can be calculated as:

$$P = g \int_0^z (\rho_b - \ \rho_{fl}) dz$$

where: g is the gravity constant; z is depth; ρ_b is the bulk density and ρ_{fl} is the fluid density.

The normal stiffness is $S_n = \frac{4\mu a}{1-PR}$. As a result, the effective Hertz-Mindlin bulk modulus (K_{HM}) of a dry, random, identical-sphere packing can be estimated as:

$$K_{HM} = \left[\frac{c^2\ (1-\emptyset)^2\ \mu^2\ P}{18\ \pi^2 (1-PR)^2}\right]^{\frac{1}{3}} \qquad (4.23)$$

If the normal force is much larger than the tangential force, $F_t << F_n$, then shear stiffness is $S_t = \frac{8a\mu}{2-PR}$. Consequently, the effective Hertz-Mindlin shear modulus (μ_{HM}) of a dry, random and identical-spheres packing is given by:

$$\mu_{HM} = \frac{5-4PR}{5(2-PR)}\left[\frac{3c^2(1-\emptyset)^2\mu^2}{2\pi^2(1-PR)^2}P\right]^{\frac{1}{3}} \qquad (4.24)$$

To determine the friction between grains contacts, the coefficient $f\,(0 \leq f \leq 1)$ is introduced, where $f = 1$ when the adhesion between grains is perfect and $f = 0$ indicates no friction. This will keep normal stiffness (S_n) constant, with the effect of the tangential stiffness to $S_t = f\frac{8a\mu}{2-PR}$. As a result, the effective Hertz-Mindlin bulk modulus stays the same and the effective shear Hertz-Mindlin modulus is given by:

$$\mu_{HM} = \frac{2+3f-PR(1+3f)}{5(2-PR)}\left[\frac{3c^2(1-\emptyset)^2\mu^2}{2\pi^2(1-PR)^2}P\right]^{\frac{1}{3}} \qquad (4.25)$$

There are different models that can calculate the dry effective bulk and shear moduli for random packing of identical elastic spherical particles at critical porosities (e.g., Walton, 1987).

The Friable or Soft-Sand (Unconsolidated) Model

Dvorkin and Nur (1996) presented the friable sand model in which the porosity decreases due to the small non-cementing particles filling the pores, which reduces porosity and increases the velocity or the stiffness of the dry rock (Figure 25). In the elastic moduli-porosity cross-plot, the high porosity end-point indicates the critical porosity and the zero-porosity end-point indicates the pure mineral, which can be a mixture of many mineral constituents (Dvorkin et al., 2014). As mentioned before, the dry effective moduli at the

critical porosity can be calculated using the Hertz-Mindlin model. This point can be connected to zero-porosity material moduli by the modified lower Hashin-Shtrikman model or the soft-sand model where effective moduli can be estimated at a different porosity as:

$$K_{soft} = \left[\frac{\phi/\phi_c}{K_{HM}+\frac{4}{3}\mu_{HM}} + \frac{1-\phi/\phi_c}{K+\frac{4}{3}\mu_{HM}}\right]^{-1} - \frac{4}{3}\mu_{HM} \qquad (4.26)$$

$$\mu_{soft} = \left[\frac{\phi/\phi_c}{\mu_{HM}+z_{HM}} + \frac{1-\phi/\phi_c}{\mu+z_{HM}}\right]^{-1} - z_{HM} \qquad (4.27)$$

where: $z_{HM} = \frac{\mu_{HM}}{6}\left[\frac{9K_{HM}+8\mu_{HM}}{K_{HM}+2\mu_{HM}}\right]$

K_{HM}, μ_{HM} are the Hertz-Mindlin - bulk and shear moduli, respectively and K is the bulk modulus of the mineral.

The Stiff-Sand Model

In the stiff-sand model (Mavko et al., 2009), the modified upper Hashin-Shtrikman (MUHS) bound describes the elastic moduli-porosity trends for clean sandstones (Dvorkin et al., 2014). Figure 26 compares the stiff-sand and soft-sand models for pure quartz grains in V_p and V_s versus porosity:

$$K_{stiff} = \left[\frac{\phi/\phi_c}{K_{HM}+\frac{4}{3}\mu} + \frac{1-\phi/\phi_c}{K+\frac{4}{3}\mu}\right]^{-1} - \frac{4}{3}\mu \qquad (4.28)$$

$$\mu_{stiff} = \left[\frac{\phi/\phi_c}{\mu_{HM}+z} + \frac{1-\phi/\phi_c}{\mu+z}\right]^{-1} - z \qquad (4.29)$$

where: $z = \frac{\mu}{6}\left[\frac{9K+8\mu}{K+2\mu}\right]$; K, μ are the bulk and shear moduli of the mineral, respectively.

The Contact-Cement Model

This model describes the velocity-porosity versus cement volume at high porosities (Figure 25). Rock in this model is highly stiffening with very little changes in porosity, which leads to rapidly increasing velocity in the rock. The contact-cement model shows the initial stage of the diagenetic trend in the data and this model is more relevant in high-porosity sands (Avseth et al., 2005). Dvorkin and Nur (1996) established the mathematical solution to estimate the effective dry-rock moduli for the contact-cement model as:

$$K_{cont-cem} = \frac{c}{6}(1 - \emptyset_c)\, M_{cem}\, S_n \qquad (4.30)$$

$$\mu_{cont-cem} = \frac{3}{5}\, K_{cont-cem} + \frac{3}{20}\, c\, (1 - \emptyset_c)\mu_{cem} S_t \qquad (4.31)$$

where: $K_{cont\text{-}cem}$ and $\mu_{cont\text{-}cem}$ are the effective bulk and shear moduli of the cemented aggregate, respectively. c is the coordination number and ϕ_c is the critical porosity. M_{cem}, μ_{cem} are the compressional and shear moduli of the cement, respectively. S_n and S_t are variables defined in the following relations:

$$S_n = A_n(\Lambda_n)\alpha^2 + B_n(\Lambda_n)\alpha + C_n(\Lambda_n);\ \ S_t = A_t(\Lambda_t, v)\alpha^2 + B_t(\Lambda_t, v)\alpha + C_t(\Lambda_t, v);$$

$$A_n(\Lambda_n) = -0.024153\ \Lambda_n^{-1.3646};\ B_n(\Lambda_n) = 0.20405\ \Lambda_n^{-0.89008};$$

$$C_n(\Lambda_n) = 0.00024649\ \Lambda_n^{-1.9864};$$

$$A_t(\Lambda_t, v) = -10^{-2}(2.26v^2 + 2.07v + 2.3)\ \Lambda_t^{0.079v^2+0.1754v-1.342};$$

$$B_t(\Lambda_t, v) = (0.0573v^2 + 0.0937v + 0.202)\ \Lambda_t^{0.0274v^2+0.0529v-0.8765};$$

$$C_t(\Lambda_t, v) = 10^{-4}(9.654v^2 + 4.945v + 3.1)\ \Lambda_t^{0.01867v^2+0.4011v-1.8186};$$

$$\Lambda_n = \frac{2\mu_c(1-v)(1-v_{cem})}{\pi\mu\ (1-2v_{cem})};\quad \Lambda_t = \frac{\mu_{cem}}{\pi\mu};\quad \alpha = \left[\frac{2(\emptyset_c - \emptyset)}{3(1-\emptyset_c)}\right]^{0.5}$$

where: v, v_{cem} are the Poisson's ratio of grain and cement minerals, respectively. μ, μ_{cem} are the shear modulus of grain and cement minerals, respectively. α is the amount of the contact cement.

The Constant-Cement Model

This model is representing the consolidated sands geological scenario (Avseth et al., 2005). Mathematically, the constant-cement model is a combination of the contact-cement and friable-sand models. The porosity reduces from the initial sand-pack at ϕ_c (Figure 25) to porosity-ϕ_b (open white circle in Figure 25). In general, it is possible to reach the constant – cement line by moving along friable-sand line and then adding contact cement to the rock (gray dashed line in Figure 25). To use this model one must first determine the well-sorted end-point porosity-ϕ_b then use contact-cement model to calculate the dry-rock bulk and shear moduli (K_b and μ_b, respectively) at ϕ_b. The effective dry-rock bulk and shear moduli for porosity less than ϕ_b can be calculated using the modified lower Hashin-Shtrikman model as:

$$K_{const} = \left[\frac{\phi/\phi_b}{K_b + \frac{4}{3}\mu_b} + \frac{1 - \phi/\phi_b}{K + \frac{4}{3}\mu_b}\right]^{-1} - \frac{4}{3}\mu_b \qquad (4.32)$$

$$\mu_{const} = \left[\frac{\phi/\phi_b}{\mu_b + z} + \frac{1 - \phi/\phi_b}{\mu + z}\right]^{-1} - z \qquad (4.33)$$

where:

$z = \frac{\mu}{6}\left[\frac{9K + 8\mu}{K + 2\mu}\right]$; K, μ are the minerals bulk and shear moduli, respectively.

In the constant-cement model, porosity reduction in sand is due to cementation where cement deposition has two certain schemes, which relates the amount of the contact cement *(α)* to the porosity of cemented sand.

Mavko et al., (2009) defined the two different schemes (Figure 27) where in scheme 1, cement deposits at grain contacts (equation 4.34) and in scheme 2, cement deposits on the grain surface (equation 4.35):

$$Scheme\ 1)\ \alpha = 2\left[\frac{\phi_c - \phi}{3c(1 - \phi_c)}\right]^{1/4} \qquad (4.34)$$

$$Scheme\ 2)\ \alpha = \left[\frac{2(\phi_c - \phi)}{3(1 - \phi_c)}\right]^{1/2} \qquad (4.35)$$

where:

ϕ_c is critical porosity, c is coordination number and ϕ is porosity.

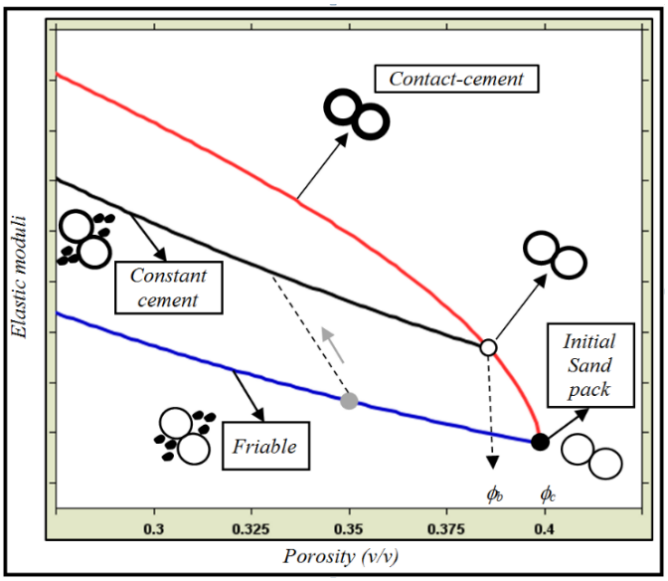

Figure 25. Elastic moduli vs. porosity plane that shows the three effective-medium models used in this study (Avseth, 2005).

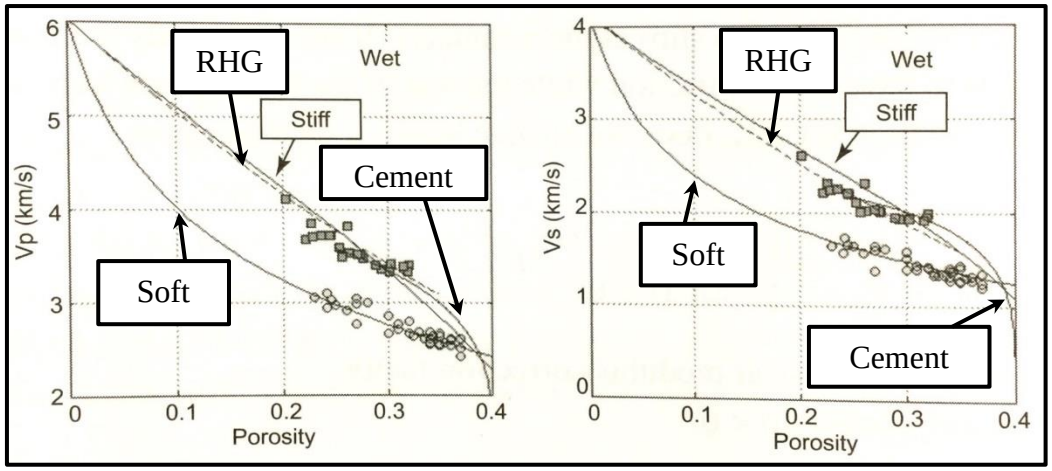

Figure 26. Velocities vs. porosity in wet rock. Wet-rock data acquired using Gassmann's fluid substitution with water bulk modulus 2.25 GPa and density 1 g/cc. Squares symbols data are from the Strandense dataset and the gray circles are from Blangy's dataset (Dvorkin et al., 2014).

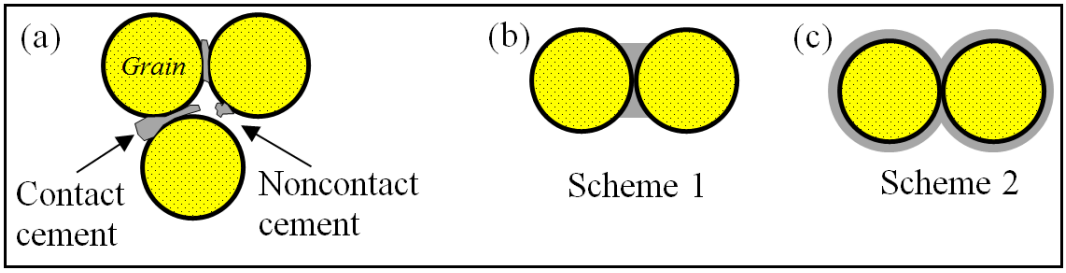

Figure 27. (a) Schematic illustration of the types of cement deposition. (b) Cement deposits at grain contact. (c) Cement deposits on the grain surface (Mavko et al., 2009).

4.3 Methodology

This section is describing the main methodologies used in this study.

4.3.1 Shear Velocity Prediction

The shear wave velocity is missing in wells 411_03 and 411_05. Therefore, the modified Gassmann's and Greenberg and Castagna techniques are used to generate missing shear velocities at the reservoir level. Mavko et al. (1995) presented fluid substitution using compressional velocity-only that operates on the compressional or *P*-modulus ($M=V_p^2\,\rho$) instead of the bulk modulus. This substitution method is known as the modified Gassmann's equation:

$$\left.\begin{aligned} M_{sat} &\approx M_s \frac{\emptyset\, M_{dry} - (1+\emptyset) K_{fl} \frac{M_{dry}}{M_s} + K_{fl}}{(1-\emptyset) K_{fl} + \emptyset\, M_s - K_{fl} \frac{M_{dry}}{M_s}} \\ M_{dry} &\approx M_s \frac{1-(1-\emptyset)\frac{M_{sat}}{M_s} - \emptyset\, \frac{M_{sat}}{K_{fl}}}{1+\emptyset - \emptyset \frac{M_s}{K_{fl}} - \frac{M_{sat}}{M_s}} \end{aligned}\right\} \qquad (4.36)$$

where: $M_{sat} = V_{p_{sat}}^2\, \rho_{sat}$; M_s is the *P*-wave modulus of solid; K_{fl} is fluid bulk modulus and ϕ is porosity.

4.3.2 Matrix (Solid) Phase

The matrix frame usually includes more than one mineral and each mineral has its own elastic properties. The ideal solution to deal with this situation is to create a single elastic property that honors all constituent elastic mineral properties. There are many ways to mix several pure minerals with their known volumetric fractions. I used Voigt (equation 4.10), Reuss (equation 4.11) and Voigt-Reuss-Hill average (equation 4.12) to calculate the matrix moduli.

4.3.3 Fluid Properties

Seismic parameters in a reservoir strongly affect by pore fluid properties. Batzle and Wang (1992) provided an empirical and theoretical model to calculate the fluid properties of the three main types of pore fluids: gas, oil and brine. I used this model to estimate the fluid properties of different phases individually.

4.3.4 Fluid Mixing

The saturation patterns in this study are recognized as homogenous. Therefore, the effective bulk modulus of this mixture of fluids is described by Wood's average:

$$\frac{1}{K_f} = \frac{f_w}{K_w} + \frac{f_o}{K_o} + \frac{f_g}{K_g} \qquad (4.37)$$

where: K_f is the effective bulk modulus of fluid. K_w, K_o and K_g are water, oil and gas bulk moduli, respectively. f is the volume fractions of the fluid phases ($f_w+f_o+f_g=1$).

4.3.5 Fluid Substitution

Gassmann modeling (Gassmann, 1951) is used to substitute different fluids. Usually, fluid substitution starts with the initial set of velocities (V_{p1} and V_{s1}) and density ρ_1, which represent the in-situ rocks with initial fluids called fluid$_1$. The common workflow for fluid substitution is described by Avseth et al. (2005):

Step 1: Calculate the in-situ bulk and shear moduli from compressional and shear sonic, and density logs as follows:

$$K_{sat1} = \rho_1 \left(V_{p1}^2 - \frac{4}{3} V_{s1}^2 \right); \quad \text{and} \quad \mu_{sat1} = \rho_1 V_{s1}^2$$

Step 2: Apply Gassmann's equation to transform the bulk modulus:

$$\frac{K_{sat2}}{K_s - K_{sat2}} - \frac{K_{fl2}}{\phi(K_s - K_{fl2})} = \frac{K_{sat1}}{K_s - K_{sat1}} - \frac{K_{fl1}}{\phi(K_s - K_{fl1})}$$

where:

K_{sat1} and K_{sat2} are the rock bulk moduli saturated with fluid$_1$ and fluid$_2$, respectively. K_{fl1} and K_{fl2} are the bulk moduli of the fluids.

Step 3: The shear modulus is:

$$\mu_{sat1} = \mu_{sat2}$$

Step 4: Correct the bulk density for the fluid:

$$\rho_{sat2} = \rho_{sat1} + \phi(\rho_{fl2} - \rho_{fl1})$$

Step 5: The new velocities with new fluid are:

$$V_{P_{sat2}} = \sqrt{\frac{(K_{sat2} + \frac{4}{3}\mu_{sat2})}{\rho_{sat2}}}; \qquad V_{S_{sat2}} = \sqrt{\frac{\mu_{sat2}}{\rho_{sat2}}}$$

4.3.6 Elastic Bounds

The Voigt-Reuss and Hashin-Shtrikman bounds between the solid and fluid endpoints are calculated and used to define the physical limits of different minerals and fluid mixtures. The upper modified Hashin-Shtrikman bound is also used with critical porosity (ϕ_c) equal to 0.4.

4.3.7 Rock Physics Model and Template

Some of the contact theory models, e.g., friable-sand, stiff-sand, contact-cement and constant-cement models (Mavko et al., 2009) were tested and evaluated at the reservoir

level. The stiff-sand model proved to be the most appropriate and universal transform for the wells data. This model was re-generated the V_p, V_s and ρ properly compare to the measured logs at the wells location. Therefore, the stiff-sand model is used and constrained by local geological conditions to build a rock physics template (RPT).

4.4 Results and Discussion

4.4.1 Shear Velocity Prediction

The first task after data conditioning, QC and reservoir properties estimation is predicting shear velocity. Therefore, the Greenberg and Castagna, (1992) method is used to predict V_s at the reservoir level in wells 411_03 and 411_05. The predicted V_s in both wells are consistent and show high correlation with the measured shear velocities in the other two wells (Figure 28).

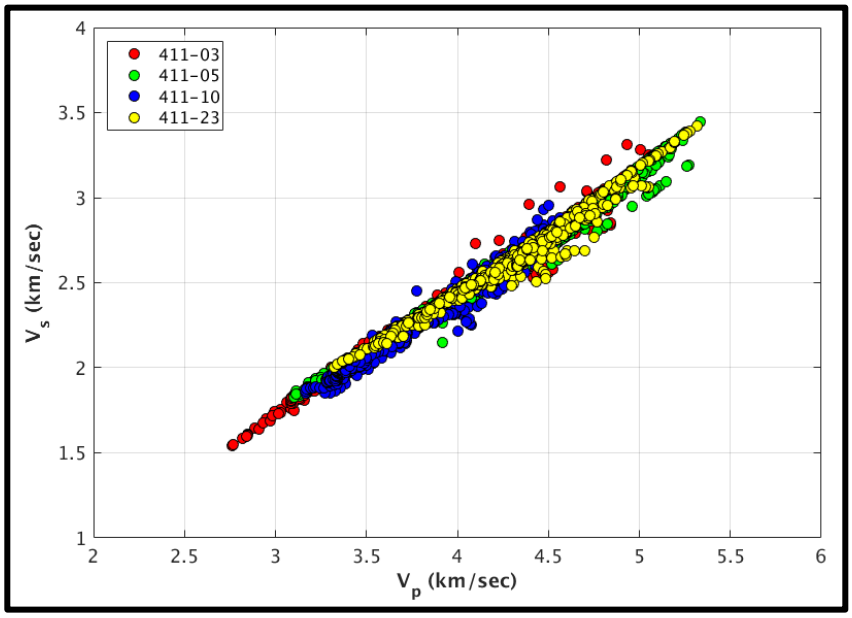

Figure 28. Comparison between predicted and measured shear wave velocities in all wells. The Greenberg and Castagna (1992) method was used to predict V_s in wells 411_03 and 411_05.

4.4.2 QC Data

The next step after *Vs* prediction in the rock physics analysis in this study is QC of the elastic logs. Figures 29 to 32 present the available and predicted logs versus depth for all wells. The dominant lithology among these wells is sandstone; there is a small amount of shale as gamma ray logs show. Quality of the reservoir is varying between wells and the average porosity is 13-16%. The shallow and deep intervals show poor reservoir quality while intermediate intervals represent good quality. The deep interval in well 411-23 is most likely water-filled.

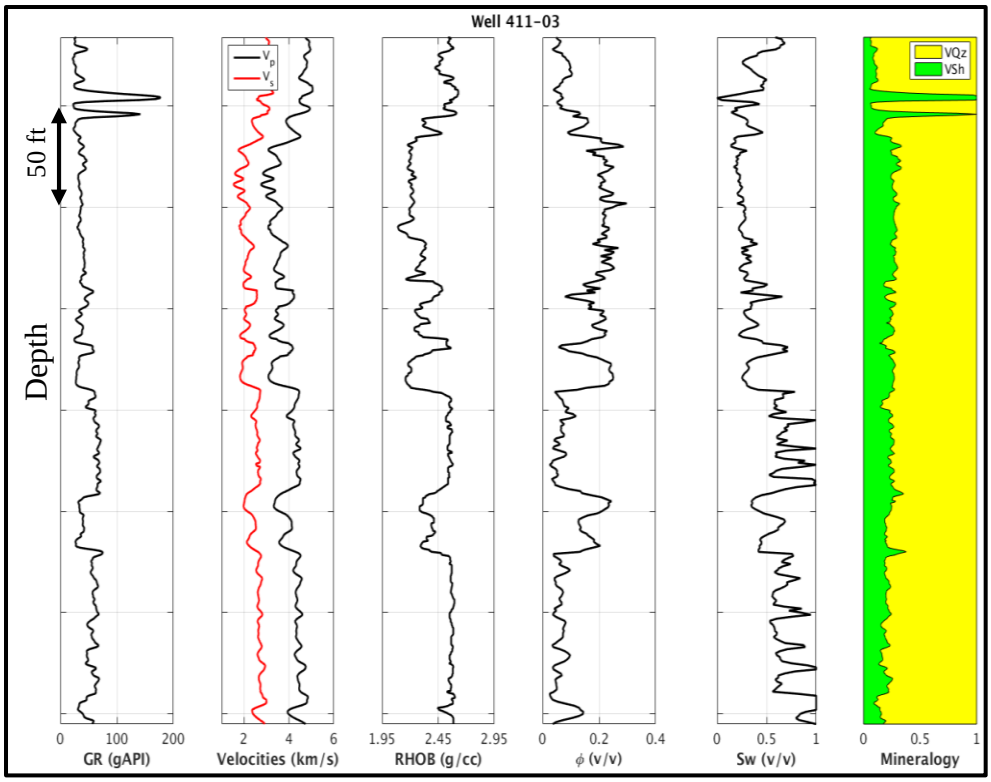

Figure 29. Available logs in well 411_03. Tracks from left to right. 1st gamma ray, 2nd V_p and V_s, 3rd density, 4th porosity, 5th water saturation and 6th mineralogy.

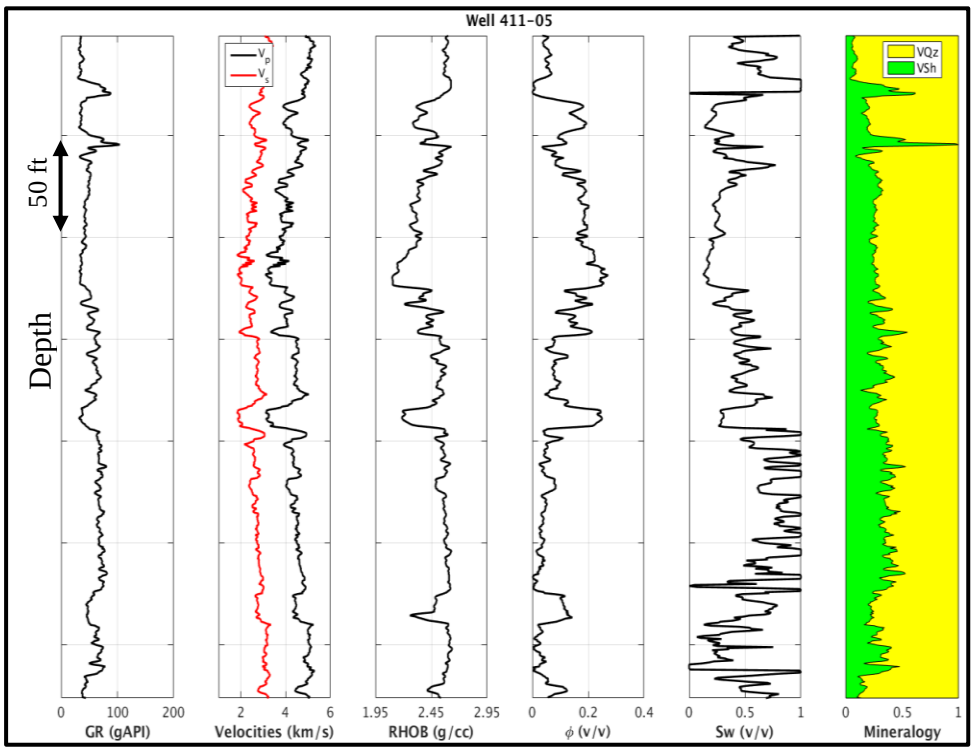

Figure 30. Available logs in well 411_05. Tracks as described in Figure 29.

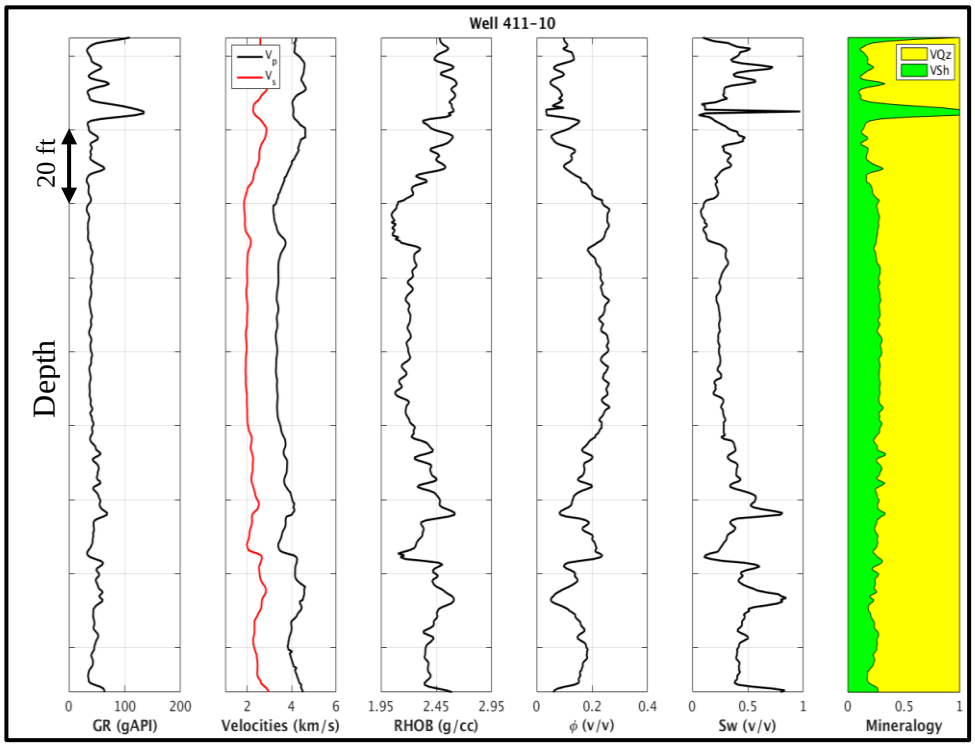

Figure 31. Available logs in well 411_10. Tracks as described in Figure 29.

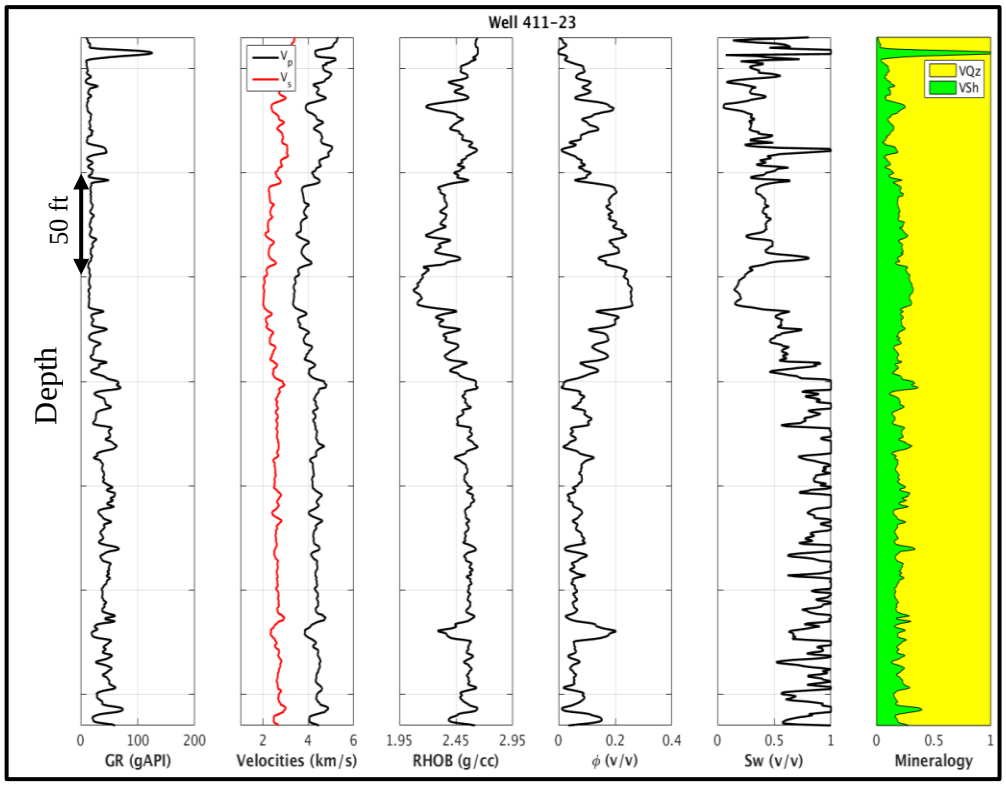

Figure 32. Available logs in well 411_23. Tracks as described in Figure 29.

Creating a relation between the elastic and reservoir properties is also a robust tool that assists to QC logs quality. In many rock physics projects, the best QC tool is a cross-plot with the simplest domains to understand the reservoir condition being the *P*-wave versus *S*-wave (V_p-V_s domain) and *P*-wave versus density (V_p-*RHOB* domain).

Using *P*-wave velocity alone is not enough to separate lithology because of the overlap in rock velocities. Adding *S*-wave information to *P*-wave data may help to understand rock composition and to reduce the uncertainty in lithology identification. In our case, and at

the reservoir level, the V_p-V_s cross-plot (Figure 33) did not add significant information because the reservoir lithology is most likely mono-mineral and semi-pure sandstone.

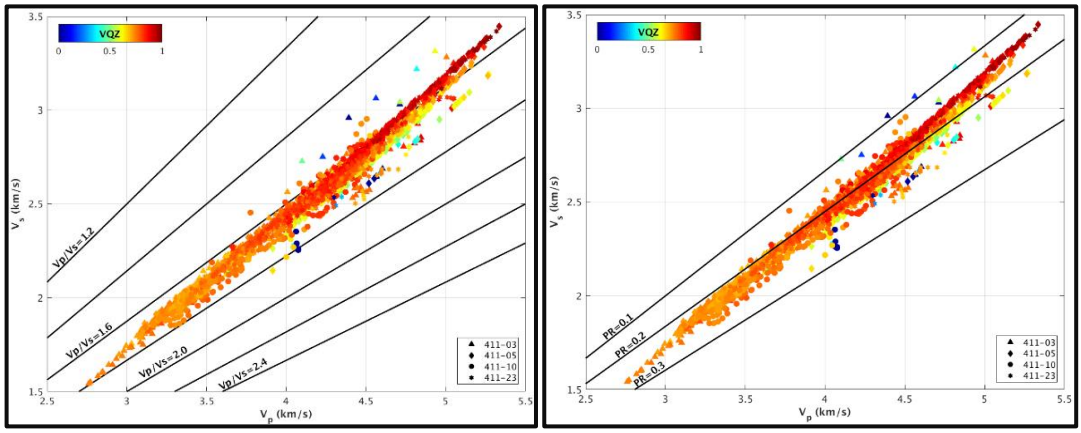

Figure 33. V_p vs. V_s cross-plots, data color-coded by volume of Quartz. Cross-plot in the left superimposed by V_p/V_s curves and in the right superimposed by Poisson's ratio curves.

V_p-*RHOB* domain is often used as a good indicator for porosity, saturation and lithology.

The low density and velocity, which is equivalent to low *P*-impedance, usually indicates high porosity as displayed in Figure 34. The same cross-plot is also used as a saturation indicator, where data is color-coded by water saturation. This type of reservoir characterized as a consolidated or stiff-sand reservoir (I will discuss this later in more detail), the effect of saturation on both velocity and density plane is usually smaller than the effect of porosity. Therefore, interpretation for fluid saturation could be difficult. Figure 35 shows that most of the hydrocarbon zone exists in low acoustic impedance intervals. It also shows hydrocarbon presence in high acoustic impedance intervals.

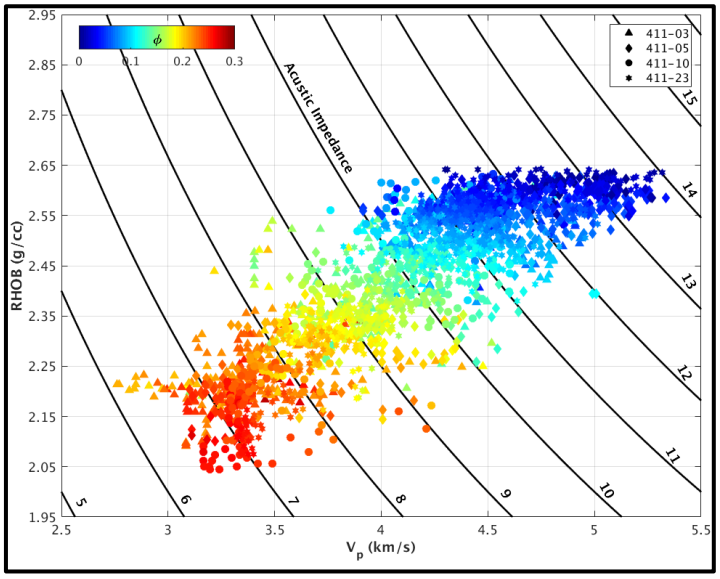

Figure 34. V_p vs. density for all wells color-coded by porosity and superimposed by constant curves of acoustic impedance.

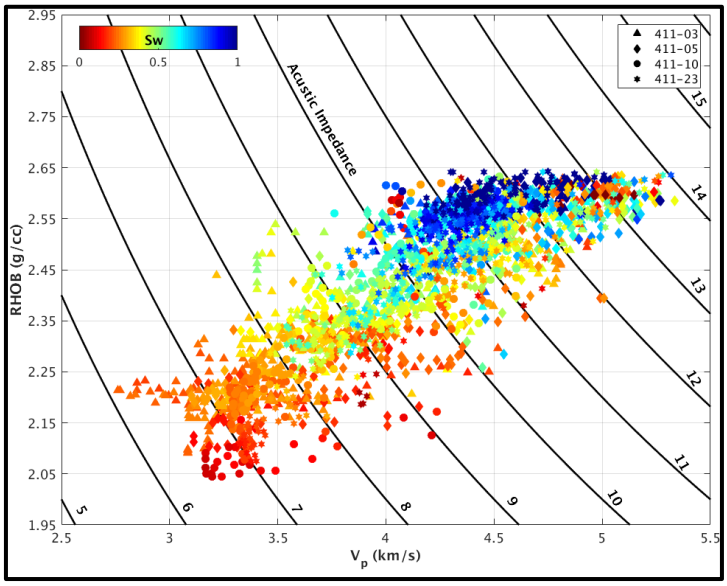

Figure 35. V_p vs. density for all wells color-coded by water saturation and superimposed by constant curves of acoustic impedance.

The porosity versus acoustic impedance cross-plot (ϕ-I_p domain) can often reveal the type and history of the digenesis. Good quality rock is located at high porosity and low I_p, but this does not necessarily represent the hydrocarbon saturation as in the current case (Figure 36), where the data from hydrocarbon-saturated intervals is broadly distributed along the porosity axis.

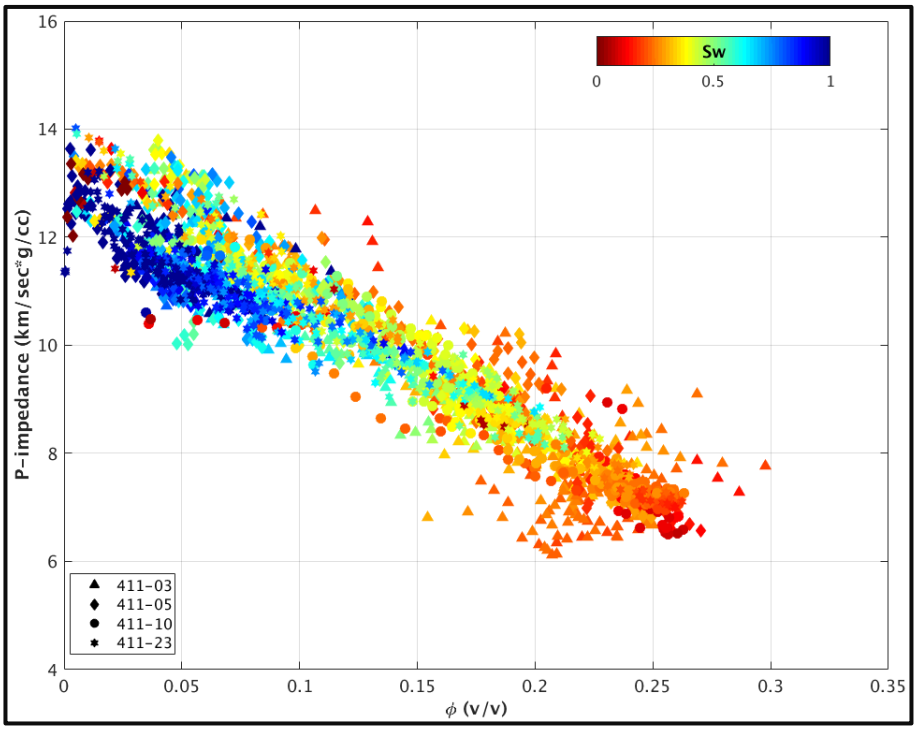

Figure 36. Porosity vs. acoustic impedance for all well, color-coded by water saturation.

Finally, the acoustic impedance versus velocity ratio cross-plot (*Ip*-V_p/V_s domain) is a good indicator for lithology, rock quality, and saturation. Low *Ip* and V_p/V_s usually indicates high-quality data and hydrocarbon zones. In our case, the sensitivity of *Ip*-V_p/V_s to saturation is significant in high porosity zones but it is less sensitive in medium to low porosity zones (Figure 37). In contrast, the porosity cut-off is evident in the acoustic impedance attribute where I can separate the high porosity from low at *Ip*=9 (km/s*g/cc), (Figure 38).

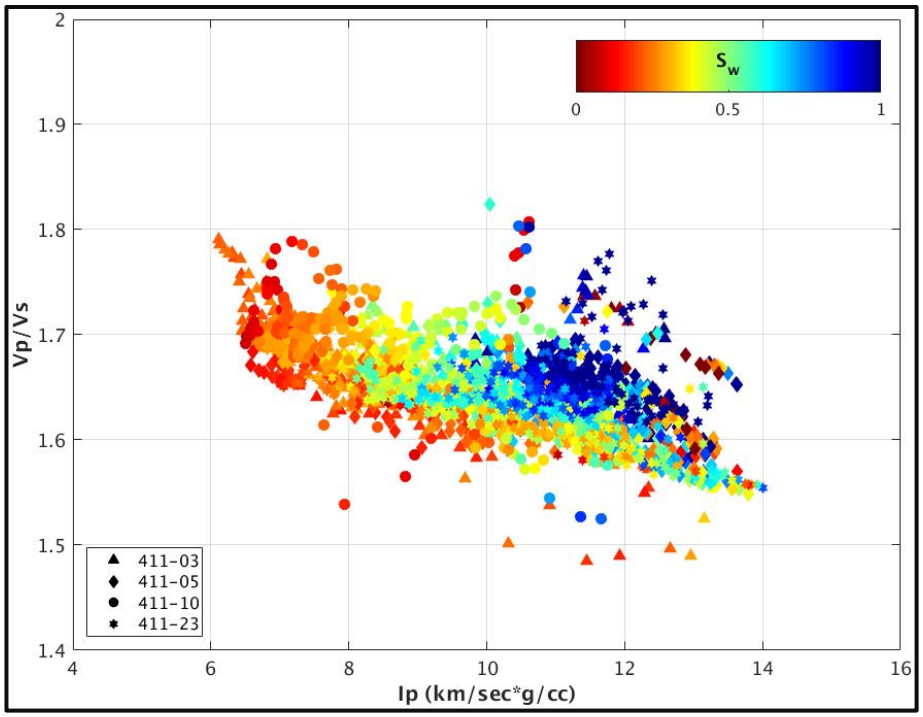

Figure 37. Acoustic impedance vs. V_p/V_s for all wells, color-coded by water saturation.

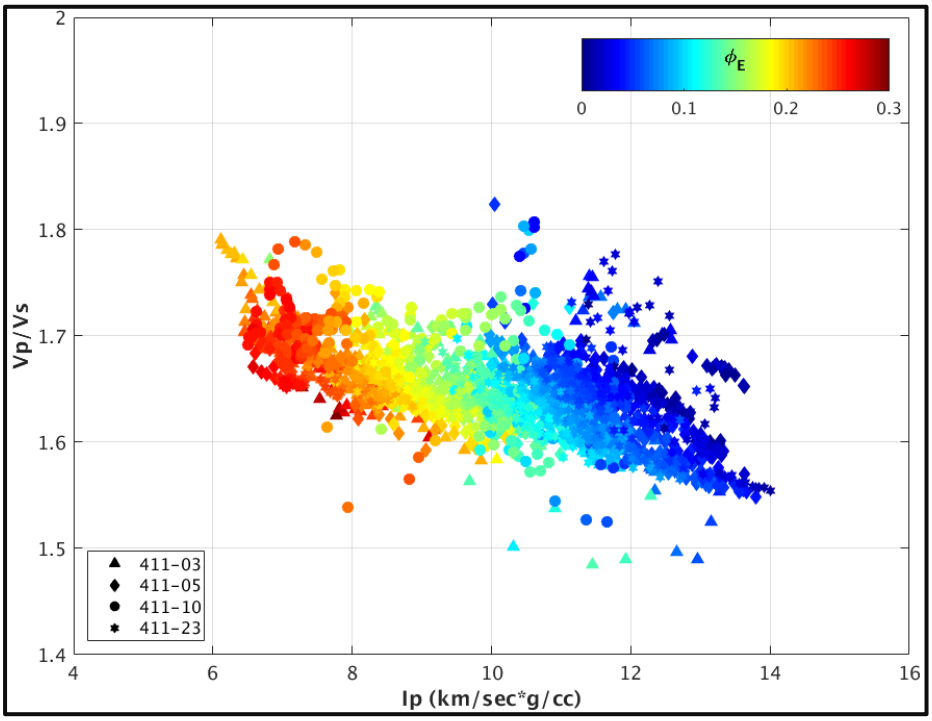

Figure 38. Acoustic impedance vs. V_p/V_s for all wells, color-coded by porosity.

4.4.3 Matrix (Solid) Phase Averaging and Elastic Bounds

As I concluded from the previous section and the lithology interpretation logs, the solids matrix in the reservoir is a mixture between only quartz and shale. The elastic bounds, which gives an idea about the physical limit of different minerals mixture, are used to QC the data. As displayed in Figure 39, the Voigt-Reuss bounds between the solid and fluid endpoints and upper modified Hashin-Shtrikman bounds with various critical porosities from 0.1 to 1, are superimposed by the in-situ bulk modulus-porosity data for each well all are color-coded by depth. The measured data for all wells falls within the bounds limit.

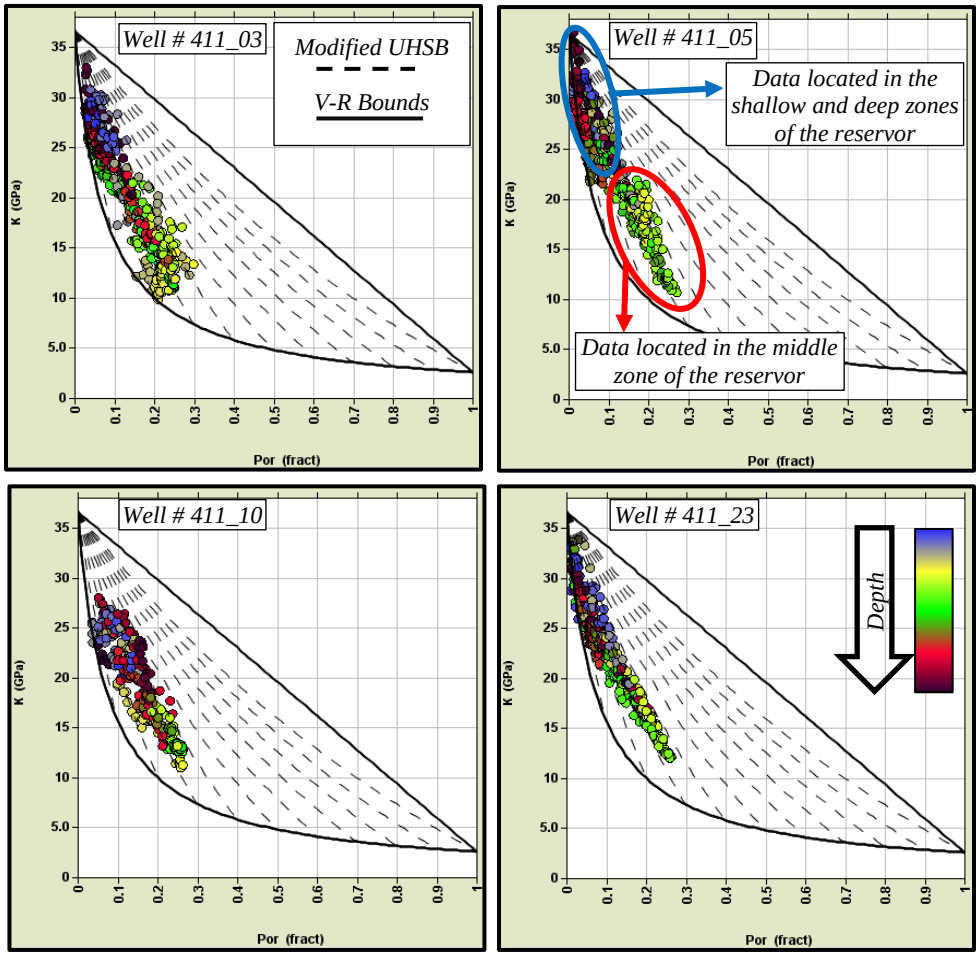

Figure 39. Voigt-Reuss and upper Hashin-Shtrikman bounds with different critical porosities varying from 0.1 to 1, superimposed by the measured data on *K*-ϕ plane, color-coded by depth.

Gamma ray (GR) measurement is used as a lithology indicator in oil/gas exploration. Therefore, the in-situ well data color-coded by GR (Figure 40) indicates that sandstone correlates to low GR and shale to high GR readings. The cross-plots in Figures 39-40 clearly indicate that the critical porosity (ϕ_c) in the reservoir is 0.4.

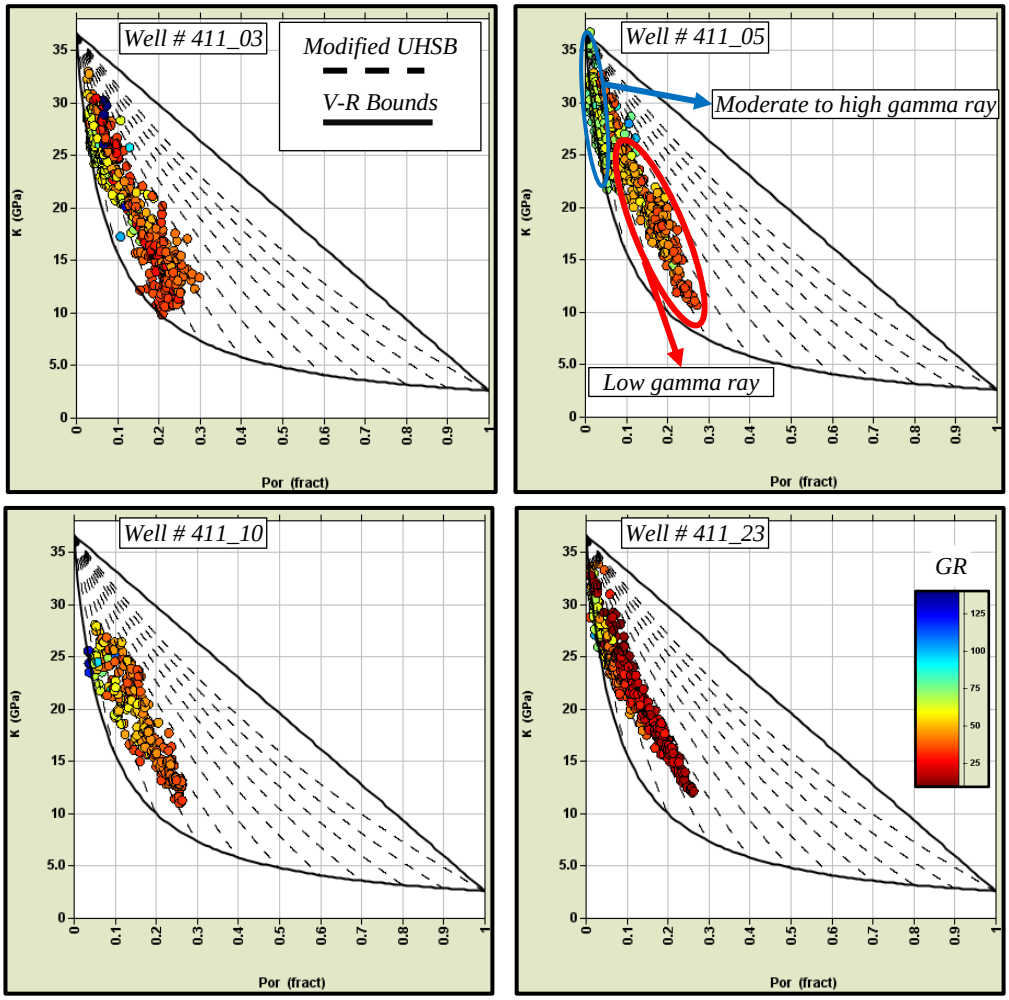

Figure 40. Voigt-Reuss and upper Hashin-Shtrikman bounds with different critical porosities varying from 0.1 to 1, superimposed by the measured data on *K*-ϕ plane, color-coded by gamma ray.

The average porosity in the reservoir varies between high and low. In some zones of both the shallow and deep intervals of the reservoir, porosity is small. In contrast, in the middle interval of the reservoir, porosity indicates the high quality data (Figure 39).

Using the modified Hashin-Shtrikman bounds (MHSB) with appropriate a minerals end point and critical porosity (0.4) will assist us to QC the data softness and stiffness in the reservoir. The bulk modulus versus porosity cross-plot (K-ϕ domain) including MHSB and measured-data in Figure 41 shows that data is falling over or near the upper MHSB, which therefore characterizes the data as stiff.

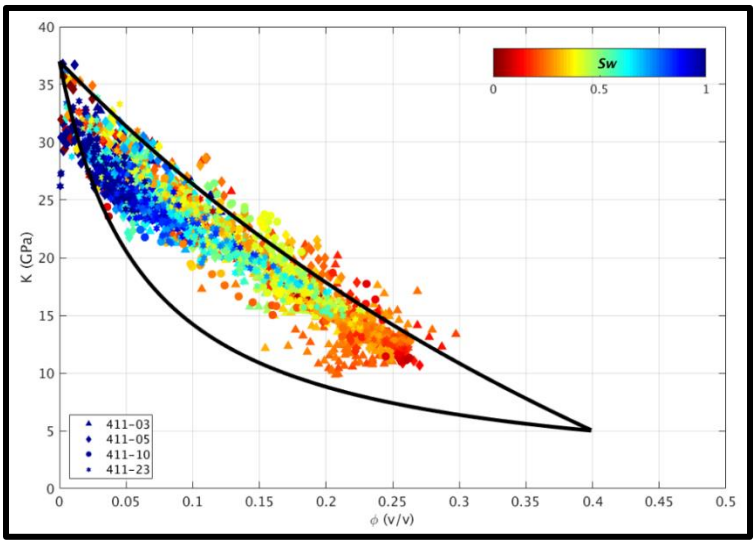

Figure 41. The upper and lower modified Hashin-Shtrikman bounds *at* ϕ_c=0.4 superimposed by the in-situ data on K-ϕ domain, data color-coded by water saturation.

4.4.4 Fluid Mixing

The Batzle and Wang (1992) model is used to estimate fluid properties. The input and output of fluid properties are listed in Table 6.

Table 6. The input and output of the fluid properties as calculated by Batzle and Wang (1992).

Input		Output		
Pressure (psi)	9,200		Water	Gas
Temperature (°F)	292	Bulk modulus (GPa)	2.8095	0.190
Salinity (ppm)	199,000	Velcoity (m/s)	1604.6	778.7
Gas gravity	0.8	Bulk density (g/cc)	1.0911	0.314

The effective bulk modulus of the hydrocarbon and water system in this study was calculated using Wood's (harmonic) average (equation 4.37). The fluid mixture result between water and gas is presented in Figure 42. The presence of small amounts of gas in the fluid system can have a very significant effect on elastic properties behavior. In our case, the presence of 5-10% gas in the fluid system reduces the bulk modulus rapidly.

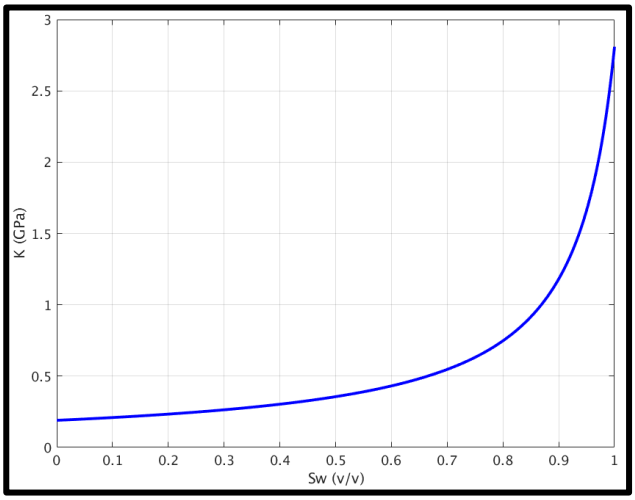

Figure 42. Fluid mixture result calculated by Wood's equation between water and gas in *Sw-K* domain.

4.4.5 Fluid Substitution

After predicting shear velocities and determining solid and fluid properties, the conventional Gassmann's model was applied in three different scenarios: 100% water saturated, 90% gas and 10% water, and 80% oil with 20% water. Figures 43 to 46 present the in-situ and modeled logs calculated by Gassmann's equation. The three different scenarios are displayed in different colors: blue logs for water, red logs for gas, green logs for oil and black logs for the in-situ. At the reservoir level, the hydrocarbon is mainly gas. This can be concluded by comparing the in-situ case (black logs) with gas case (red logs) where they overlay each other over the reservoir.

The separation between the three scenarios is significant in different elastic attributes (e.g., V_p/V_s, Poisson's ratio, Lambda-rho and Lambda/Mu) especially in the high porosity zones.

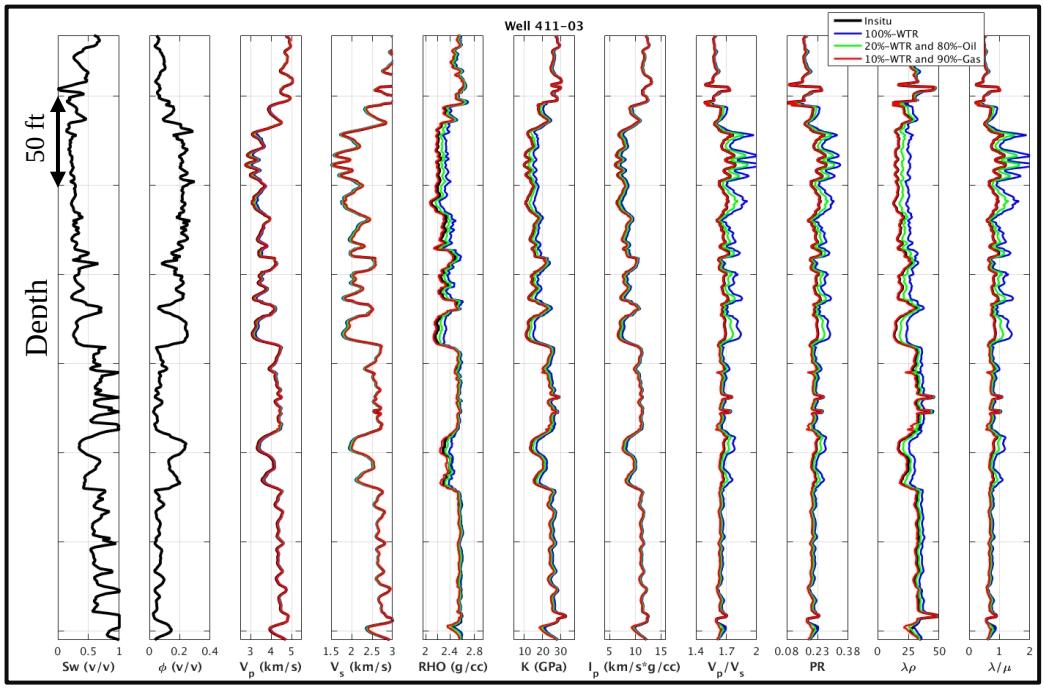

Figure 43. Gassmann's model result for well 411_03 (blue curves for water, red for gas, green for oil and black for in-situ). Tracks from left to right: saturaion, porosity, V_p, V_s, density, bulk modulus, acoustic impedance, V_p/V_s ratio, Possion's ratio, lambdaRho and lambda/Mu.

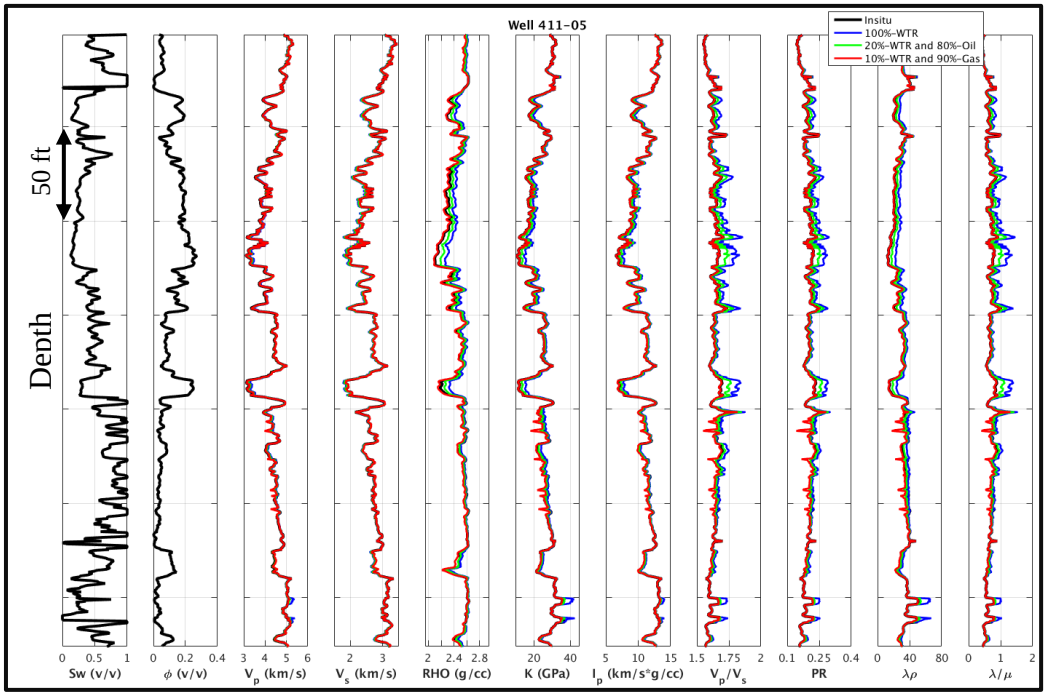

Figure 44. Gassmann's model result for well 411_05. Tracks as described in Figure 43.

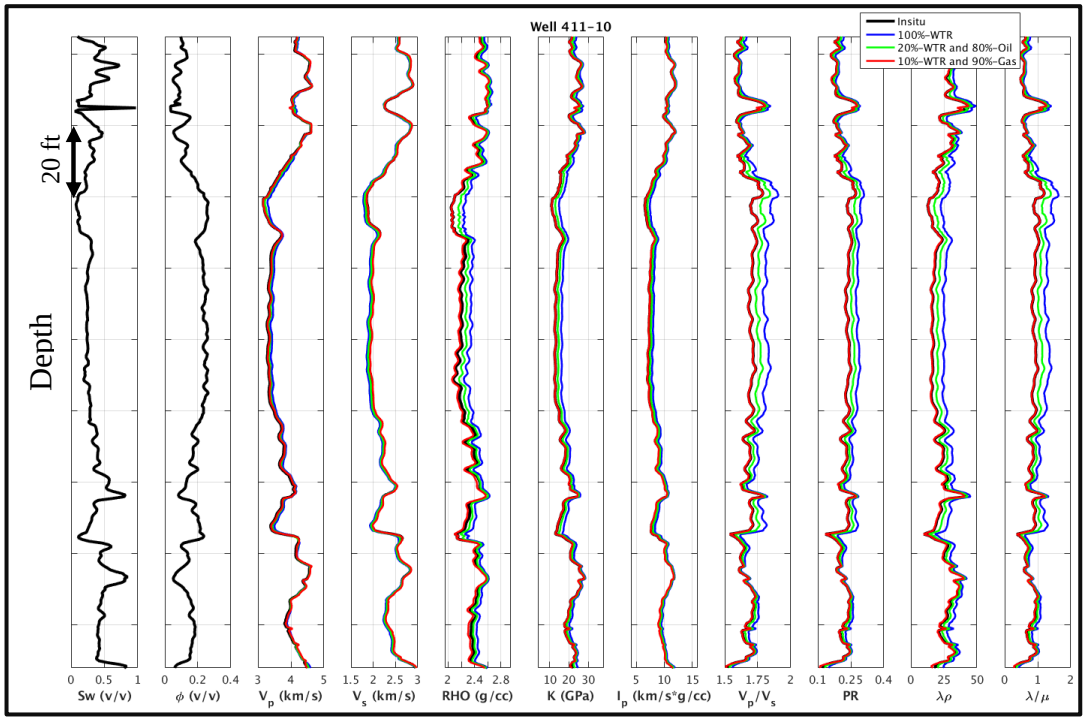

Figure 45. Gassmann's model result for well 411_10. Tracks as described in Figure 43.

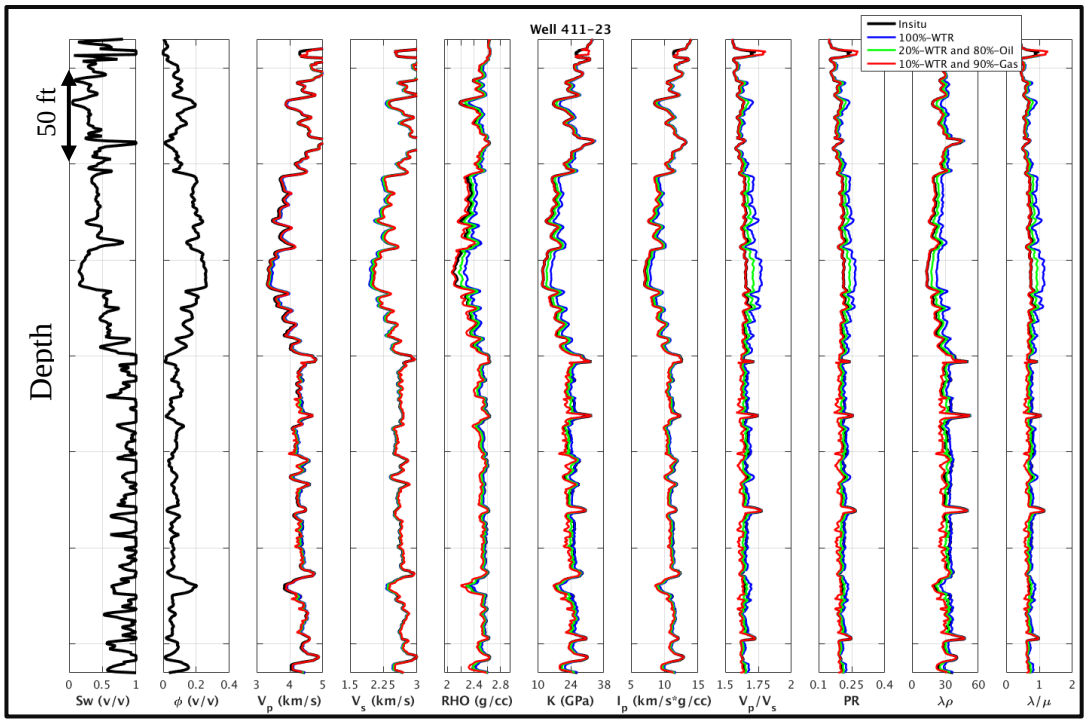

Figure 46. Gassmann's model result for well 411_23. Tracks as described in Figure 43.

The results of Gassmann's fluid substitution in the porosity versus bulk modulus (ϕ-K) domain are shown in Figure 47. In this domain, fluids separation does not appear in the low/medium porosity zones and small separation in the bulk modulus is noticed in the high porosity zones.

In the acoustic impedance and velocity ratio domain (Figure 48), the separation between different fluid scenarios is noticeable, especially in the high porosity zone. In the low acoustic impedance direction, porosity increases and hydrocarbon-saturation increases in the low velocity ratio directions. The sensitivity of V_p/V_s ratio to different fluids is generally remarkable but in our case, the changes in V_p/V_s between fluid types is only significant in high porosity zones.

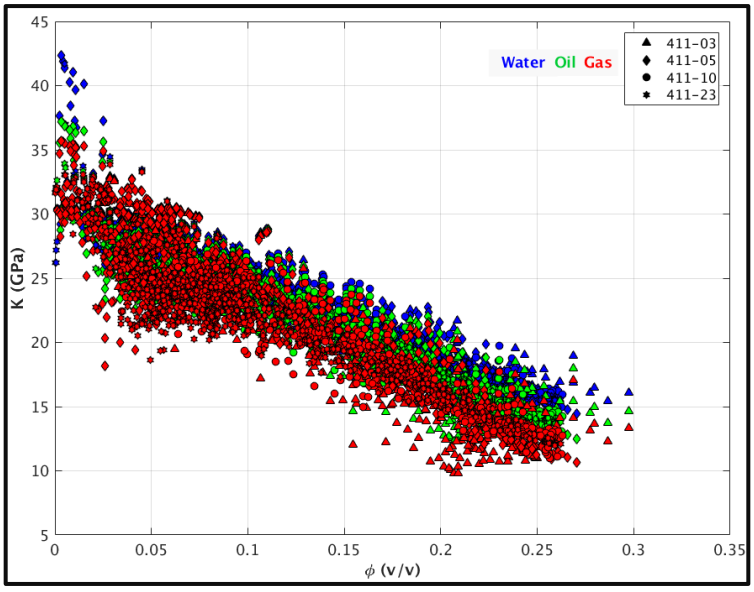

Figure 47. Porosity vs. bulk modulus for three different fluid scenarios in all wells.

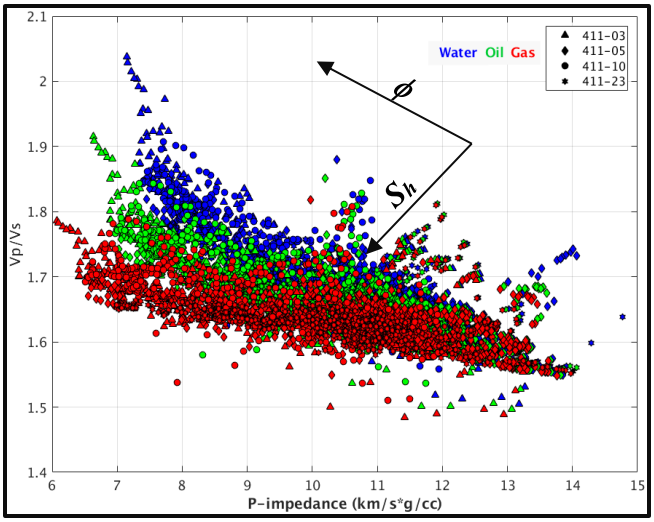

Figure 48. Acoustic impedance vs. V_P/V_S for three different scenarios in all well.

4.4.6 Rock Physics Model and Template

There are many rock physics models that endeavor to link rock elastic properties to reservoir properties (Dvorkin et al., 2014). To find an appropriate rock physics model, I first conducted fluid substitution for 100% wet conditions to eliminate the fluid effect. Next, I cross-plotted porosity versus wet V_p and V_s and evaluated and tested various models to match the data (Figure 49).

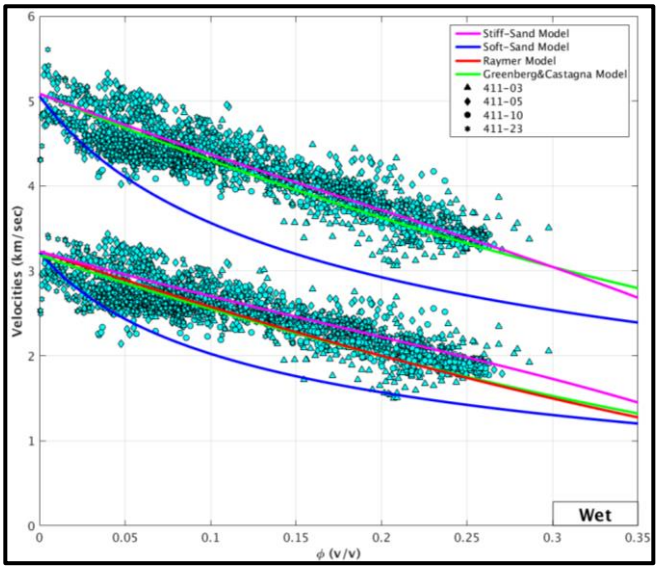

Figure 49. Porosity vs. velocities cross-plot includes wet data for all wells superimposed by stiff-sand, soft-sand models and V_S predictors, including Raymer and Greenberg and Castagna's models.

Many rock physics models were evaluated including stiff-sand model (Mavko et al., 2009), soft-sand model (Dvorkin and Nur, 1996), Raymer et al. (1980) model for V_p and combined with different V_s predictors, including Raymer-Dvorkin (2008), as well as Greenberg and Castagna (1992) models. The conclusion from this evaluation and testing flow is that the stiff-sand model is the most appropriate model for honoring the in-situ data at the reservoir level (Figure 50).

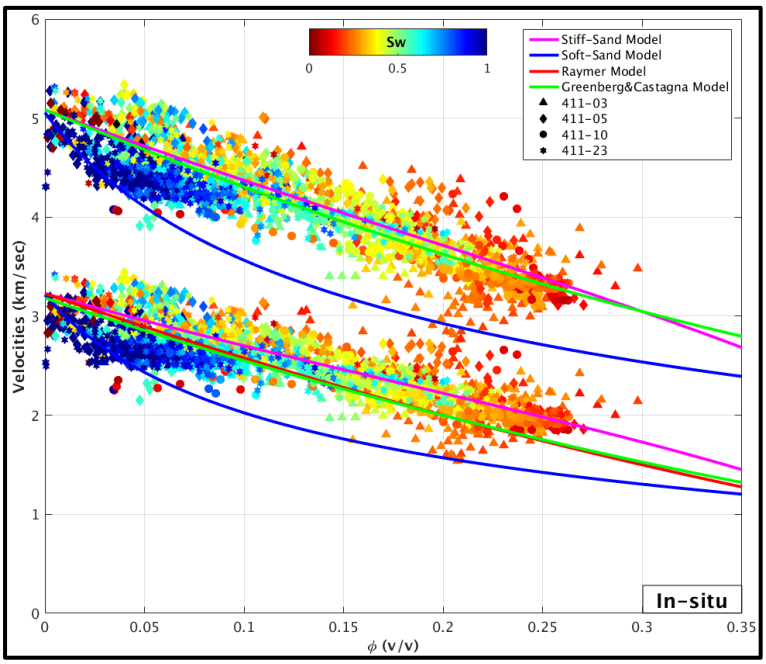

Figure 50. Porosity vs. velocities cross-plot includes in-situ data for all wells superimposed by stiff-sand, soft-sand models and V_s predictors, including Raymer and Greenberg and Castagna's models.

The stiff-sand model selected in this study connects the two end points in the modulus-porosity plane with the modified upper Hashin-Shtrikman bound (Mavko et al., 2009). At the zero-porosity endpoint, I used the average of the mix minerals between quartz and shale. At the high-porosity endpoint (i.e., critical porosity), the elastic moduli are given by the Hertz-Mindlin contact theory (Mavko et al., 2009). This model was used with a critical

porosity of 0.4, coordination number of 9, shear correction factor of 1 and a differential pressure of 25 MPa.

One of the powerful tools for efficient lithology and pore-fluid interpretation of well-log data and elastic inversion is the Rock Physics Template (RPT). The most common form of the RPT is a lithology and fluid indicator, which is described by the cross-plot of V_p/V_s ratio versus *acoustic impedance*. The RPT is also used to verify the applicability of the selected model. First, I created the RPT using the model-based data, color-coded by porosity (Figure 51) and color-coded by volume of quartz (Figure 52), then superimposed the in-situ data from all wells in the same figures. I obtained an almost perfect match between the in-situ data and model in the porosity domain. In addition, the in-situ data-points fairly well match the RPT in lithology domain but deviate from it in some intervals. One reason for this mismatch may be due to data quality. Another reason for this apparent miss-match may be refer to assumptions and estimated values that were used in the thesis work steps (e.g., the reservoir lithology, fluid properties and Archie's water saturation parameters). In general, there are so many factors affecting the elastic properties of the rocks and their relation to petrophysical properties; furthermore, there is no physical/mathematical model that can exactly predict the behavior of each data point. Instead, I aim at a reasonable physical-based model that explains the trends observed in the data and, so can be used in interpreting elastic logs for petrophysical properties.

The next step in my analysis is to verify the accuracy of our model prediction at the well locations. First, I conducted forward modeling in each well to predict velocities and densities: the results are presented in Figures 53 to 56. While the matches between the

measured and modeled logs are quite good in most of the reservoir intervals in all wells, the match is still far from perfect in some intervals.

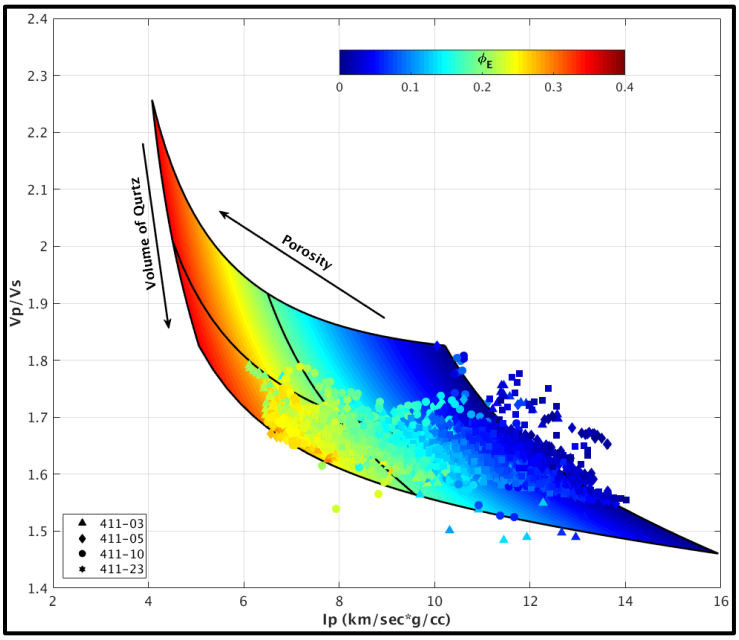

Figure 51. Stiff-sand RPT in acoustic impedance vs. velocity ratio over-imposed by in-situ data and color-coded by porosity.

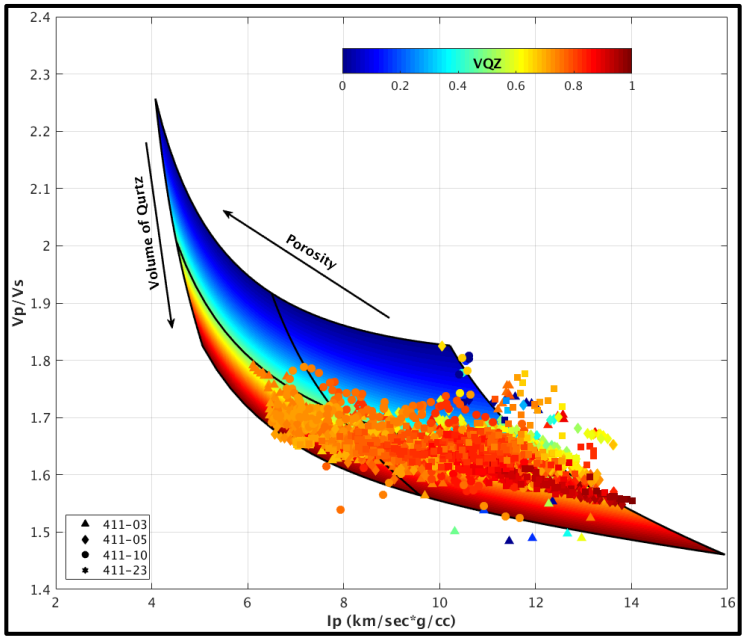

Figure 52. Stiff-sand RPT in acoustic impedance vs. velocity ratio over-imposed by in-situ data and color-coded by volume of quartz.

In some zones, the model overestimated velocities in the low porosity intervals and underestimated velocities in the high porosity intervals. These mismatches may be due to the lack of accurate information and thus missed in petrophysical properties estimation, as discussed earlier. Spikes appeared in the modeled velocities in 100% shaly intervals. The model failed to predict the velocity response in these zones because I used an approximation of the shale properties, which do not accurately represent the real shale properties. Therefore, the absence of this information (e.g., fluid properties, shale properties, etc.) reduces quality and accuracy of the model prediction.

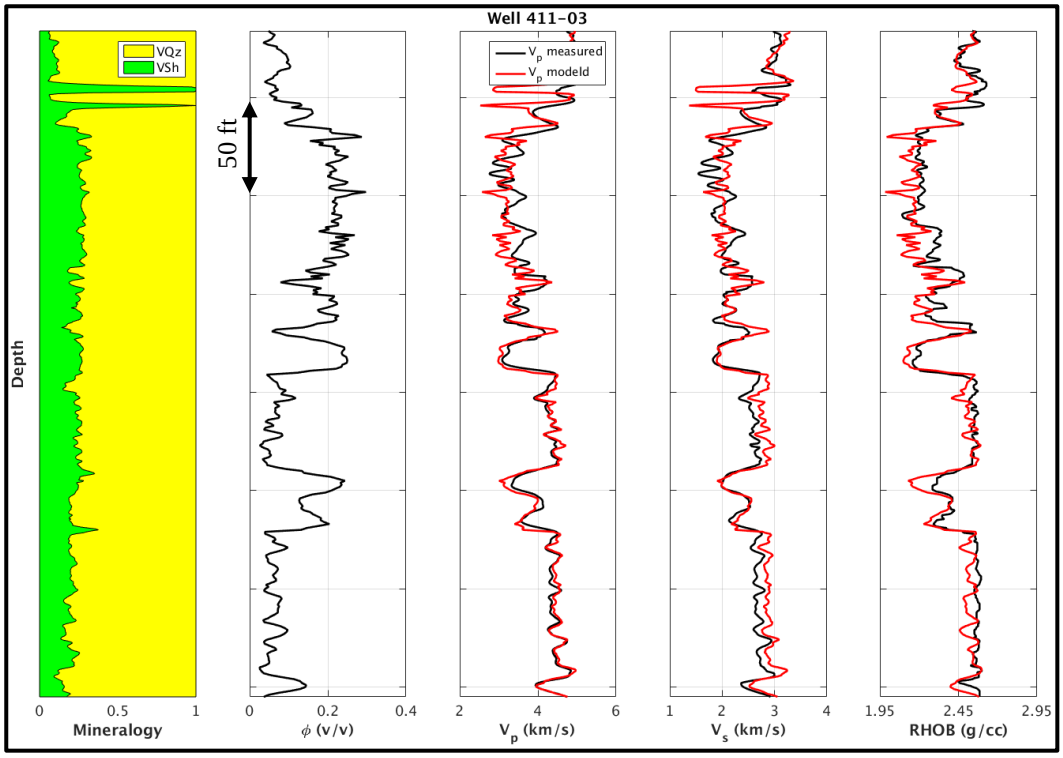

Figure 53. The elastic modeled-data using stiff-sand model in well 411_03. Tracks from left to right: mineralogy, porosity, V_p, V_s and density. In the last three tracks black logs are measured and red logs are modeld.

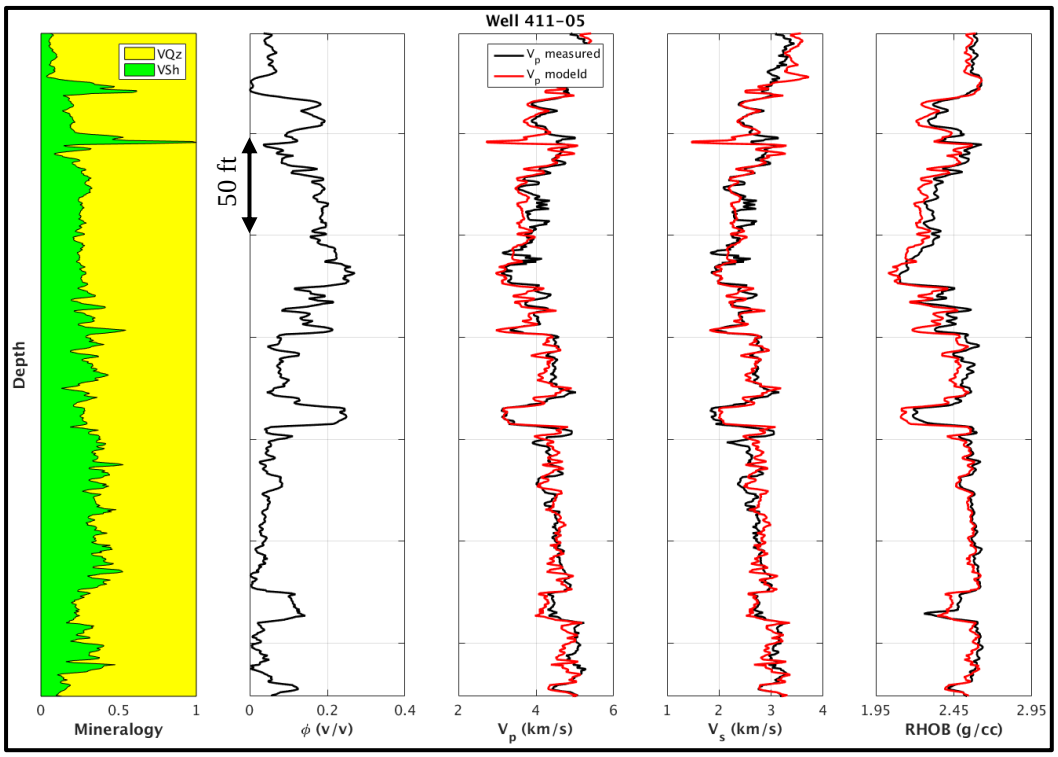

Figure 54. The elastic modeled-data using stiff-sand model in well 411_05. Tracks as described in Figure 53.

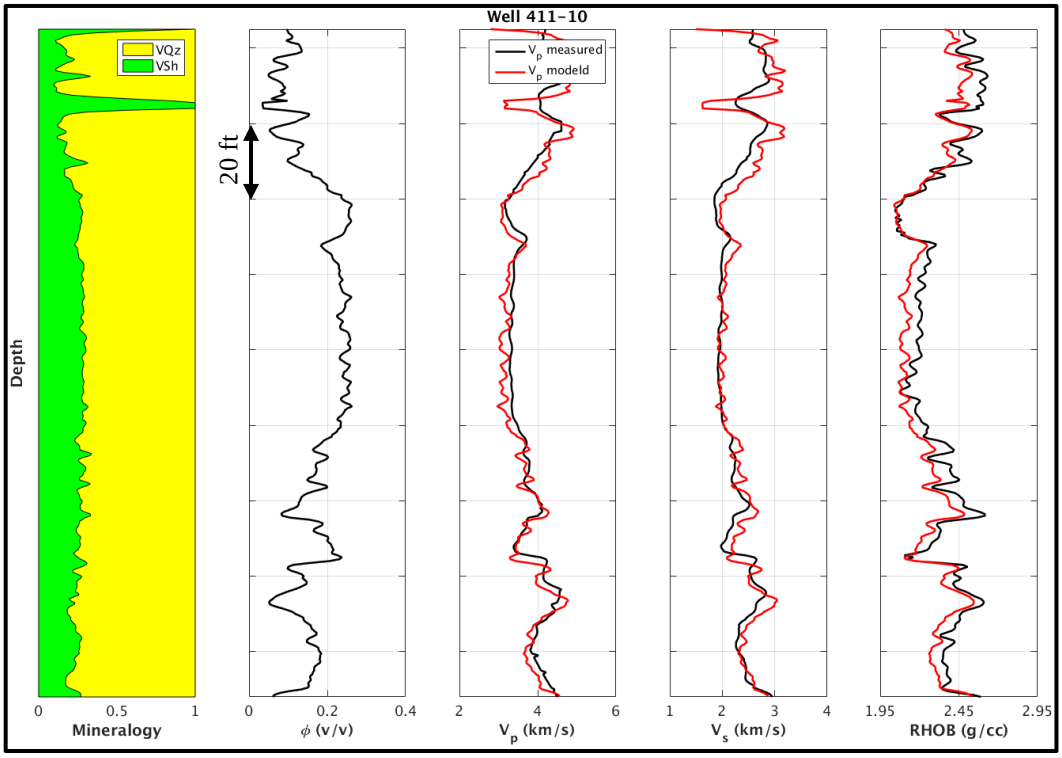

Figure 55. The elastic modeled-data using stiff-sand model in well 411_10. Tracks as described in Figure 53.

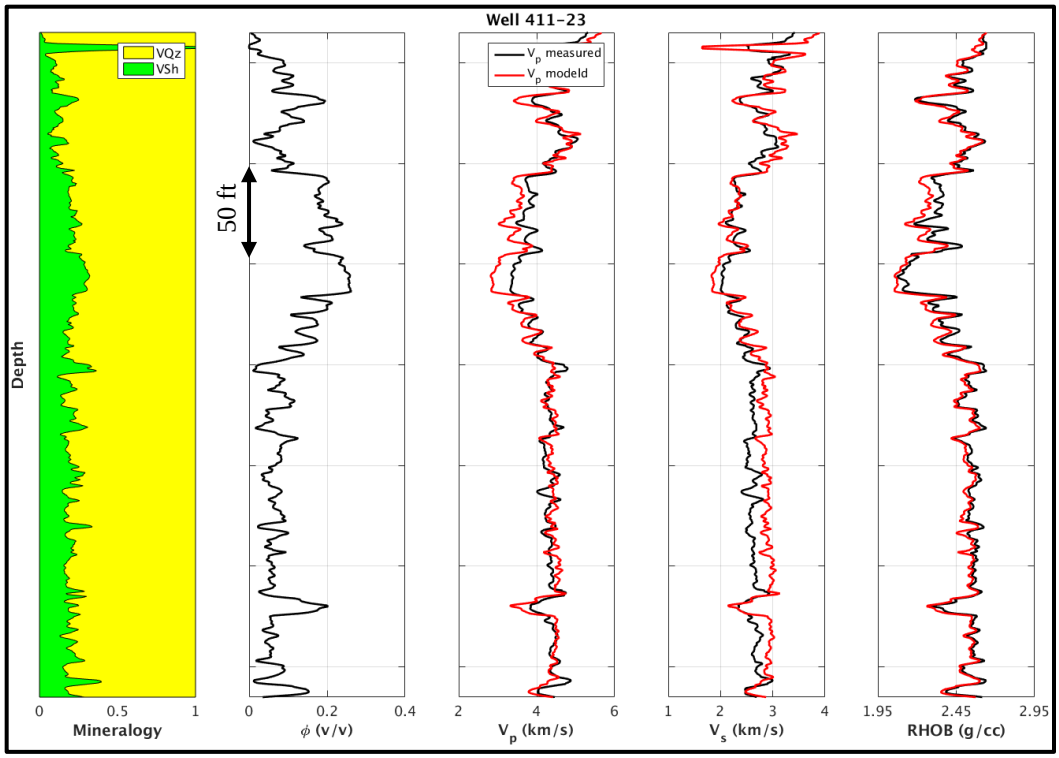

Figure 56. The elastic modeled-data using stiff-sand model in well 411_23. Tracks as described in Figure 53.

After evaluating the accuracy of the model predication, I established and verified the rock physics model based on the in-situ data at the well locations. The next step was to use the model with seismic-based elastic attributes, such as the acoustic impedance, to predict petrophysical rock properties. Because in this case, the mineral in the reservoir was the same (most likely sandstone) and the sensitivity to the pore-fluid was quite small, I concentrated on obtaining porosity from seismically derived impedance. Hence, to relate the porosity to measured impedance I used the best second-order polynomial fit (equation 4.38) to describe the model and its mean (Figure 57):

$$\emptyset = 0.001\, \mathrm{I}_p^2 - 0.0609\, \mathrm{I}_p + 0.6355\,; \qquad R^2 = 0.9 \qquad (4.38)$$

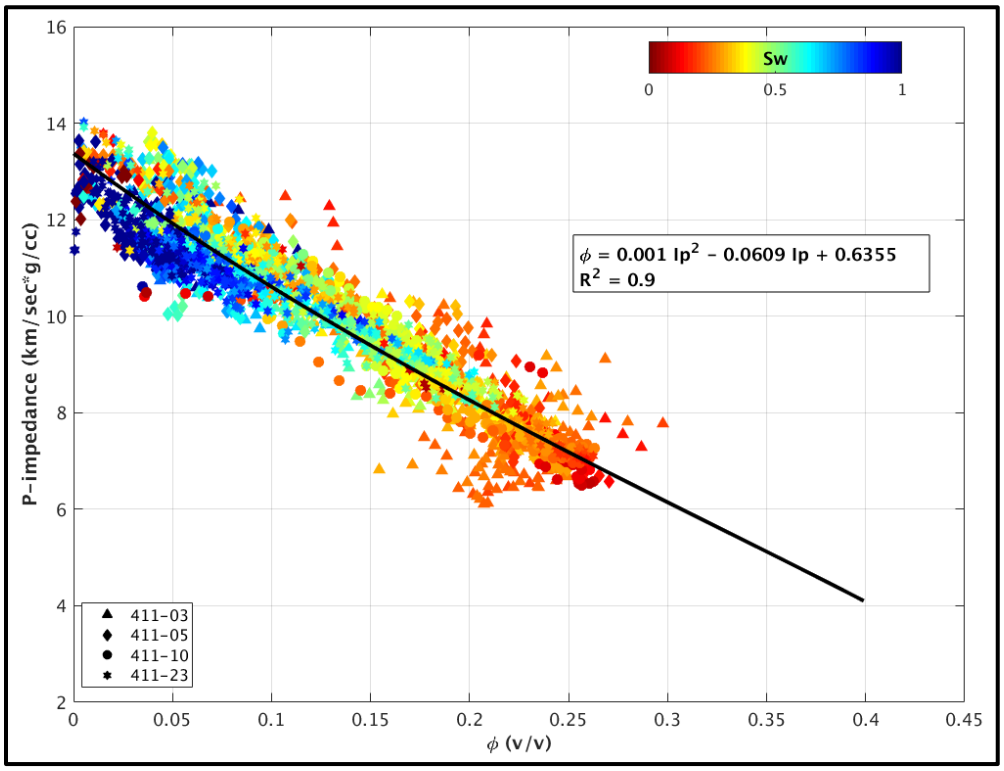

Figure 57. The porosity vs. acoustic impedance includes in-situ data for all wells with the fitting model equation superimposed upon the data.

CHAPTER 5

CONCLUSIONS

5.1 Summary

In this study, four wells in a clastic reservoir were used to build a rock physics model and a diagnostic rock physics template. Each well had a set of reservoir depth interval logs including caliper, gamma ray, resistivity, bulk density, as well as compressional and shear sonic logs. Different methods were adopted to condition the elastic logs and to predict missing sections. The petrophysical properties were calculated using the available logs and reservoir information. Archie's equation was used to calculate the water saturation. For computation of mineral volumes, a deterministic method was used with no core calibration.

Many quality control techniques were used in this study to confirm the petrophysical results, which were later incorporated into the rock physics analysis and modeling. One important step of rock physics analysis (rock physics diagnostics) is to bring the entire intervals under examination to the so-called common fluid state, which means that the elastic properties were computed for a 100% wet condition. With this target in mind, the Batzle and Wang, (1992) method was used to calculate fluid properties. Then Gassmann's equation (Gassmann, 1951) was used to estimate the elastic properties for full water saturation and for different fluid saturation scenarios in the reservoir. The fluid substitution

results showed that the in-situ fluid in the reservoir was most likely gas or gas mixed with water.

At the reservoir level, several rock physics models were tested and evaluated, including Raymer's (1980), the Greenberg and Castagna (1992), soft-sand model (Dvorkin and Nur, 1996) and stiff-sand model (Mavko et al., 2009). The stiff-sand model, constrained by local mineral grain properties and adjusted to the local geology, proved to be the most appropriate model for use in this study. As a result, this model should be used for further quantitative seismic interpretation.

5.2 Recommendations

The limited number of wells and lack of lithology and fluid properties information were the main challenges in this study. Therefore, including cores, thin sections, known fluid properties, adding more wells and wireline logs such as neutron and Photoelectric Factor (PEF) will improve the results and reduce uncertainties. A sensitivity analysis is recommended in order to evaluate the effect of some missing data such as shear velocity on my models and analyses.

It would also be extremely useful to apply the workflows designed in this study to other wells in the same field to test the sensitivity and quality of the model developed for this reservoir. It is also very important to use the best quality data available while implementing these workflows. It is recommended that researchers extrapolate the reservoir properties away from the well location, by inverting seismic data constrained by the rock physics models.

Finally, because the non-reservoir rock properties affect seismic data, in the future I need to address relations between them using theoretical rock physics models. Once again, to reach the ultimate goal of rock physics analysis successfully, I need to have high-quality data logs for the reservoir.

References

[1] Avseth, P.; Mukerji, T.; Mavko, G.; Quantitative Seismic Interpretation. *Cambridge, Cambridge University Press, 2005.*

[2] Bakhorji, A.; "Laboratory Measurements of Static and Dynamic Elastic Properties in Carbonate," *Ph.D. dissertation, University of Alberta, 2010*.

[3] Batzle, M.; Wang, Z.; "Seismic properties of pore fluids," *Geophysics, vol.57, no.11, pp. 1396-1408, Nov 1992.*

[4] Burch, D.; "Seismic to well ties with Problematic Sonic Logs," *AAPG Explorer, Part 1 Feb, Part 2 Mar 2002*.

[5] Castagna, J.; Batzle, M.; and Kan, T.; "Rock physics – The link between rock properties and AVO response," In *Offset – Dependent Reflectivity – Theory and Practice of AVO Analysis. Investigation of Geophysics, No. 8, SEG, pp. 135-171, 1993.*

[6] Clavier, C.; Hoyle, W.; Meunier, D.; "Quantitative interpretation of thermal Neutron decay time logs: Part I. fundamentals and techniques," *SPE paper 6859, in 52nd annual technical conference and exhibition, June 1971.*

[7] Dvorkin, J.; "Yet another V_s equation," *Geophysics, 73, E35-E39, 2008a.*

[8] Dvorkin, J.; Nur, A.; "Elasticity of high-porosity sandstones: theory for two North Sea datasets," *Geophysics, vol.61, no.5, pp. 1363-1370, Sep 1996*

[9] Dvorkin, J.; Gutierrez, M.; and Grana, D.; Seismic Reflections of Rock Properties, *First Edition, Cambridge University, 2014*.

[10] Gardner, G. H. F; Gardner, L. W.; Gregory, A. R.; "Formation Velocity and Density: the Diagnostic for Stratigraphic traps," *Geophysics, vol.39, no.6, pp. 770-780, Dec 1974.*

[11] Gardner, J. S.; Dumanoir, J. L.; "Litho-Density: Log Interpretation," *SPWLA, 21st annual logging symposium, Jul 1980.*

[12] Gassmann, F.; "Uber die elastizitat poroser medien," *Vier. Natur Gesellschaft, 96, 1-23, 1951.*

[13] Greenberg, M. L.; Castagna, J. P.; "Shear-wave Velocity Estimation in Porous Rocks: Theoretical Formulation, Preliminary Verification and Applications," *Geophysics Prospecting, 40, pp. 195-209, 1992.*

[14] Gunarto, M.; Irawan, B.; "Well-log Conditioning and Rock Physics Modeling: A First Step in Seismic Reservoir Characterization," *IPA 34th Annual Convention Proceedings, May 2010.*

[15] Han, D.; Nur, A.; Morgan, D.; "Effects of Porosity and Clay Content on Wave Velocities in Sandstones," *Geophysics, vol.51, no.11, pp. 2093-2107, Nov 1986.*

[16] Hashin, Z.; Shtrikman, S.; "A variational approach to the elastic behavior of multiphase materials," *Journal of Mechanics and Physics Solids, vol.11, pp. 127–140, 1963.*

[17] Kuster, G.; ToksÖz, M.; "Velocity and attenuation of seismic waves in two-phase media Part I. Theoretical Formulations," *Geophysics, vol.39, no.5, pp. 587-606, Oct 1974.*

[18] Lakes, R.; Drugan, W.; "Dramatically stiffer elastic composite materials due to a negative stiffness phase?," *Journal of the Mechanics and Physics of Solids, vol. 50, pp.979-1009, 2002.*

[19] Mavko, G.; Chan, C.; Mukerji, T.; "Fluid substitution: Estimating changes in V_p without knowing V_s," *Geophysics, vol.60, no.6, pp. 1750-1755, Nov-Dec 1995.*

[20] Mavko, G.; Mukerji, T.; Dvorkin, J.; The Rock Physics Handbook, Tools for Seismic Analysis of Porous Media, *Second Edition, Cambridge University, 2009*

[21] Melvin, J.; Sorague, R.; Heine, C.; "From bergs to ergs: The late Paleozoic Gondwanan Glaciation and its aftermath in Saudi Arabia," *Geological Society of America Special Papers, vol. 468, p. 37-80, 2010.*

[22] Melvin, J.; Wallick, B.; Heine, C.; "Advances in Arabian stratigraphy: Allostratigraphic layering related to paleo-water table fluctuations in eolian sandstones of the Permian Unayzah A reservoir, South Haradh, Saudi Arabia," *GeoArabia, vol.15, no.2, pp. 55-86, Jan 2010.*

[23] Mindlin, R., "Compliance of elastic bodies in contact," *Journal of Applied Mechanics, vol.16, pp. 259-268, 1949.*

[24] Nur, A.; Mavko, G.; Dvorkin, J.; Galmudi, D.; "Critical porosity: A key to relating physical properties to porosity in rocks," *The Leading Edge, vol.17, pp. 357-362, Mar 1998.*

[25] Raymer, L.; Hunt, E.; and Gardner, J.; "An improve sonic transit time-to-porosity transform," *SPWLA, 21st annual logging symposium, July 1980.*

[26] Reuss, A.; "Berechnung der Fliesssgrenzen von Mischkristallen auf Grund der Plastizitatsbedingung fur Einkristalle," *Z. Ang. Math. Mech., 9, 49-58, 1929.*

[27] Rider, M.; The Geological Interpretation of Wells Logs, *Whittles Publishing. 1996.*

[28] Schlumberger; Log Interpretation Principles/Applications, *1987.*

[29] Vernik, L.; "Acoustic velocity and porosity systematics in siliciclastics," *Society of Petrophysicists & Well Log Analysts, vol.39, pp. 27-35, Jun 1997.*

[30] Voigt, W.; "Lehrbuch der Kristallphysik," *Leipzig, Berlin, B.G. Teubner, 1910.*

[31] Wallick, B.; Giroldi, L.; "Interpretation of full-azimuth broadband land data from Saudi Arabia and implications for improved inversion, reservoir characterization, and exploration," *Interpretation, vol. 1, no. 2, pp. T167-T176, Nov. 2013.*

[32] Walls, J.; "Use of Well Logs in Seismic Reservoir Characterization," *Houston Geological Society, abstract, Oct. 2004*

[33] Walton, K.; "The effective elastic moduli of a random packing of spheres," *Journal of Applied Mechanics, vol.35, pp. 213-226, 1987.*

[34] Wang, Z.; Nur, A.; Batzle, M.; "Acoustic velocities in petroleum oils," *Journal of Petroleum Technology, vol. 42, pp. 192-201, Feb 1990.*

[35] Wang, Z.; Nur, A.; "Seismic and acoustic velocities in reservoir rocks," *Society of Exploration Geophysicists, vol. 3, 2000.*

[36] Wang, Z., "Fundamentals of seismic rock physics," *Geophysics, vol.66, no.2, pp. 398-412, Mar-Apr 2001.*

[37] Western Atlas International Inc., Introduction to Wireline Log Analysis, *1992.*

[38] Wyllie, M.; Gregory, A.; and Gardner, G.; "An experimental investigation of factors affecting elastic wave velocities in porous media," *Geophysics, 20, No. 3, 459-493, July 1958.*

Vitae

Name	Omar Hussein Omar Afif
Nationality	Saudi
Date of Birth	8/14/1974
Email	omarafif@yahoo.com
Address	P.O. Box 5302
	Dhahran 31311
	Saudi Arabia
Academic Background	B.S. in Applied Geology-Geophysics,
	King Abdul Aziz University, Jiddah.

I have been working with Saudi Aramco since 2007 in different geophysics related departments. I also worked in Saudi Geological Survey (SGS) for 7 years as a geophysicist. Prior to working in SGS, I was a member of the geophysical department in USGS Mission, Jeddah, for one year in 1999. I am a member of SEG, EAGE and DGS.

Publication:

Omar, A.; Jack, D.; "Building a rock physics model for a carbonate reservoir in Saudi Arabia," SEG Technical Program Expanded Abstract 2016: pp. 3277-3281

Omar, A.; Muhammad, A.; "The impact of Geophysical Well Log Analysis (GWLA) on a clastic rock physics analysis," Geo-2016, 12th Middle East Geosciences Conference & Exhibition, Manama, Bahrain, March 7-10, 2016; Article No. 90254.

Omar, A.; Ahmed, M.; "Different approaches to shear wave prediction," Geo-2014, 11th Middle East Geosciences Conference & Exhibition, Manama, Bahrain, March 10-12, 2014; Article No. 90188.

Ahmed, M.; Omar, A.; Gupta, M. "Diagenetic and pore fluid effects on a tight clastic reservoir (a case study)," Geo-2014, 11th Middle East Geosciences Conference & Exhibition, Manama, Bahrain, March 10-12, 2014; Article No. 90188.

Ahmed, G.; Omar, A.; "Enhanced residual statics by gradually building a velocity model: a case study," Geo-2012, 10th Middle East Geosciences Conference & Exhibition, Manama, Bahrain, March 4-7, 2012; Article No. 90141.